Genome editing in the mouse brain with minimally immunogenic Cas9 RNPs

Elizabeth C. Stahl,[1,2,3] Jennifer K. Sabo,[1] Min Hyung Kang,[1,5] Ryan Allen,[1] Elizabeth Applegate,[1] Shin Eui Kim,[1] Yoonjin Kwon,[1,3] Anmol Seth,[1,3] Nicholas Lemus,[1,3] Viviana Salinas-Rios,[1] Katarzyna M. Soczek,[1,2,3] Marena Trinidad,[1] Linda T. Vo,[1,9] Chris Jeans,[2] Anna Wozniak,[4] Timothy Morris,[4] Athen Kimberlin,[4] Thomas Foti,[4] David F. Savage,[1,3,5] and Jennifer A. Doudna[1,2,3,5,6,7,8,9]

[1]Innovative Genomics Institute, University of California, Berkeley, Berkeley, CA 94720, USA; [2]California Institute for Quantitative Biosciences (QB3), University of California, Berkeley, Berkeley, CA 94720, USA; [3]Department of Molecular and Cell Biology, University of California, Berkeley, Berkeley, CA 94720, USA; [4]Aldevron LLC, Madison, WI 53719, USA; [5]Howard Hughes Medical Institute, University of California, Berkeley, Berkeley, CA 94720, USA; [6]Department of Chemistry, University of California, Berkeley, Berkeley, CA 94720, USA; [7]MBIB Division, Lawrence Berkeley National Laboratory, Berkeley, CA 94720, USA; [8]Gladstone Institutes, University of California, Berkeley, San Francisco, CA 94114, USA

Transient delivery of CRISPR-Cas9 ribonucleoproteins (RNPs) into the central nervous system (CNS) for therapeutic genome editing could avoid limitations of viral vector-based delivery including cargo capacity, immunogenicity, and cost. Here, we tested the ability of cell-penetrant Cas9 RNPs to edit the mouse striatum when introduced using a convection-enhanced delivery system. These transient Cas9 RNPs showed comparable editing of neurons and reduced adaptive immune responses relative to one formulation of Cas9 delivered using AAV serotype 9. The production of ultra-low endotoxin Cas9 protein manufactured at scale further improved innate immunity. We conclude that injection-based delivery of minimally immunogenic CRISPR genome editing RNPs into the CNS provides a valuable alternative to virus-mediated genome editing.

INTRODUCTION

Editing somatic cells directly *in vivo* is anticipated to be the next wave of therapeutics for many genetic diseases, especially those affecting the central nervous system (CNS).[1,2] Clustered regularly interspaced short palindromic repeats (CRISPR) is a revolutionary tool adapted from bacterial immune systems for genome editing.[3–5] To achieve gene disruption, the functional endonuclease, Cas9, is directed by a guide RNA to a target site in DNA to generate a double-strand break leading to insertions and deletions (indels). Unfortunately, despite many genetic disease indications, the brain remains a challenging target for genome editing.

To circumvent the blood-brain barrier (BBB), most genomic medicines rely on direct intracranial injection of viral vectors encoding the transgene of interest. Viral vectors, such as recombinant adeno-associated virus (AAV), have had great success in gene therapy and are less immunogenic than most viral vectors; however, they require re-manufacturing for each target and are hindered by costly production scale-up. In addition, AAV has a limited DNA packaging capacity, and is associated with immunogenicity in the brain from both the

vector and expression of foreign transgenes.[6–9] Although the brain has been considered an immune-privileged site, green fluorescent protein can induce a strong inflammatory response and neuronal cell death 3 weeks after injection with AAV serotype 9 has been reported.[6–9] In addition, Cas9-specific immune responses have been elicited following AAV delivery in mice[10–12] and pre-existing cellular and humoral immunity to Cas9 and AAVs are documented in humans.[13–18] Despite these drawbacks, AAVs are the most clinically relevant delivery systems currently in use for the CNS.

The development of transient, non-viral delivery systems that can effectively edit neurons throughout the brain with minimal immunogenicity would greatly facilitate future clinical applications. Previously, we developed cell-penetrating Cas9 ribonucleoproteins (RNPs) capable of genome editing in mouse neurons both *in vitro* and *in vivo*.[19] To enable self-delivery of the Cas9 RNPs, four repeats of the positively charged Simian vacuolating virus 40 nuclear localization sequences (SV40-NLS) were fused to the N terminus along with two repeats to the C terminus of Cas9, a strategy that was also reported to enable delivery of zinc-finger nucleases.[20] Using a single guide to turn on the tdTomato reporter from the lox-stop-lox Ai9 mouse,[21] we reported edited striatal volume of approximately 1.5 mm.[3,19]

Here, we report further optimization of cell-penetrant Cas9 RNPs, demonstrating efficacy in human primary cells and improved editing of the mouse striatum using a convection-enhanced delivery (CED) system. We compared the transient RNP complexes with AAV serotype 9 for Cas9 delivery to the CNS, to measure both editing efficiency and the host immune response. We found that the Cas9-AAV was
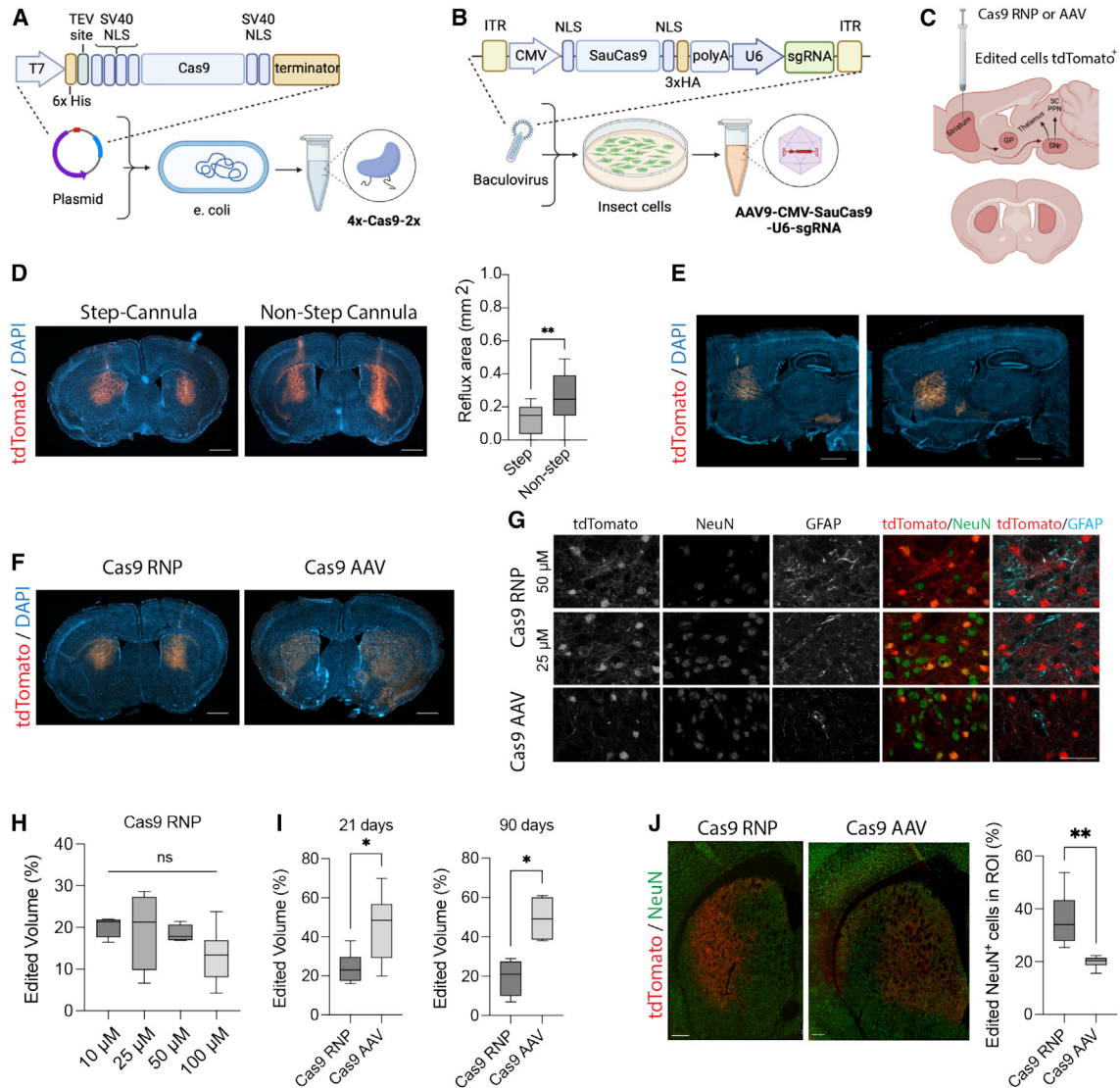
Figure 1. *In vivo* editing at tdTomato locus with viral and non-viral Cas9 delivery strategies

(A) Schematic of 4x-SpyCas9-2x cell-penetrant protein expression and purification systems, (B) AAV9-SauCas9-sgRNA expression and purification systems, and (C) expected edited brain regions in the basal ganglia shown in sagittal view (top) and coronal view (bottom). Striatal neurons extend into the globus pallidus and substantia nigra. Created with BioRender.com. (D) Comparison of convection-enhanced delivery (CED) of cell-penetrant 4x-SpyCas9-2x RNP with step and non-step cannulas (n = 3–6 injections per group, unpaired t test, **p < 0.01.) Scale bars, 1 mm. (E) Serial sections of single hemisphere sagittal view of edited tdTomato$^+$ cells in the basal ganglia circuit after injection of Cas9 RNP with CED into the striatum. Scale bar, 1 mm. (F) Representative coronal section of the striatum of mice that received Cas9 RNPs and AAVs at 21 days post-injection, showing the distribution of tdTomato$^+$ edited cells. Scale bar, 1 mm. (G) Co-staining of tdTomato with NeuN and GFAP in the striatum at 90 days post-injection. Scale bar, 50 μm. (H) Volume of edited striatal tissue as the concentration of injected Cas9 RNPs was increased from 10 to 100 μM (n = 4–6 injections, one-way ANOVA, ns). (I) Quantification of editing following treatment with Cas9 AAV (3e-9 vg/μL, 1.5e-10 vg/hemisphere) and Cas9 RNPs (25 μM, 125 pmol/hemisphere) at 21 and 90 days (n = 4–6 injections, one-way ANOVA, *p < 0.05). (J) Co-expression of tdTomato and NeuN quantified per regions of interest (ROIs), e.g., edited area per hemisphere (n = 4–6 injections, one-way ANOVA, **p < 0.01). Scale bars, 250 μm.

able to better diffuse throughout the brain, leading to distally edited cells; while the cell-penetrant Cas9-RNPs edited more neurons within the region near the injection site. Both groups elicited humoral responses, but vehicle-specific antibodies in the Cas9-AAV group persisted at higher levels out to 90 days. Cas9-AAV-treated brains were also associated with significantly elevated *Cd3e* gene expression at 4 weeks, suggesting an ongoing adaptive immune response. Cas9-RNP-treated brains showed acute microglial activation that was mitigated by reducing endotoxin levels during protein manufacturing scale-up. Taken together, Cas9 RNPs are a promising strategy for future therapeutic intervention in neurological disorders to address current limitations of viral delivery.

RESULTS

Development of Cas9 cell-penetrant RNP and AAV to measure genome editing with the tdTomato reporter system

Creating a large deletion in the lox-stop-lox cassette in Ai9 mice with a single-guide RNA (sgRNA) enables expression of tdTomato and efficient quantification of editing by fluorescent readout (Figure S1A). Cas9 from *Streptococcus pyogenes* (engineered with four copies of SV40 NLS on the N terminus and two copies on the C terminus [4x-SpyCas9-2x] to be cell penetrant) was first produced from recombinant *E. coli* in a laboratory setting, using a low endotoxin method. Editing efficiency of the RNP was compared with Cas9 delivered by recombinant AAV (Figures 1A–1C). Since SpyCas9 cannot be packaged within a single AAV with its guide RNA, we used clinically relevant AAV-SauCas9-sgRNA (derived from *Staphylococcus aureus*).[22–24] AAV serotype 9 was produced using a baculovirus transfected into Sf9 insect cells.[25,26] To control for differences in the Cas9 orthologs, cell-penetrant 4x-SauCas9-2x protein was also produced following the same expression and purification methods as 4x-SpyCas9-2x. Due to differences in PAM requirements between the two Cas9 orthologs (SpyCas9 NGG and SauCas9 NNGRRT), a new guide was designed for SauCas9 to target the tdTomato locus (Figure S1B).

We confirmed editing in neural precursor cells (NPCs) isolated from embryonic day 13.5 Ai9 mice with all constructs *in vitro* (Figure S1). Addition of 4x-SauCas9-2x RNP into the cell culture supernatant enabled editing of NPCs compared with 0x-SauCas9-2x RNPs, demonstrating that the four SV40-NLS peptides can mediate delivery of additional Cas9 orthologs. 4x-SauCas9-2x RNPs were slightly less efficacious than 4x-SpyCas9-2x RNPs, which could be explained in part by differences in the guide RNAs (Figures S1A and S1B). We observed editing of mouse NPCs with SauCas9 when delivered as both cell-penetrant RNP (59% ± 6% tdTomato cells$^+$, Figures S1C and S1D) and AAV (42% ± 1% tdTomato cells$^+$, Figure S1E). The same titer of AAV9-CMV-GFP resulted in 96% ± 2% GFP$^+$ cells, suggesting that editing lagged behind transduction; and an increase in empty capsids in the AAV-CMV-SauCas9 group was noted (Figure S1F).[27,28]

To further examine the potential for cell-penetrant Cas9 RNPs to edit difficult cells *in vitro*, we tested delivery and editing with 4x-SpyCas9-2x in human NPCs derived from induced pluripotent stem cells (iPSCs).[29–31] Human NPCs were treated with pre-formed RNPs using an established guide RNA targeting EMX1.[32] In human cells, we detected 10-fold higher rates of editing with 4x-SpyCas9-2x compared with standard RNPs (0x-SpyCas9-2x) delivered with commercial transfection reagents (Figures S2A and S2B).

Cas9 RNPs result in modest editing of brain parenchyma following delivery into cerebrospinal fluid

To determine the optimal route of delivery for Cas9 RNPs into the mouse CNS, we tested intraparenchymal injections into the striatum, as well as injection into the cerebrospinal fluid (CSF), including intrathecal (i.t.) and intracerebroventricular (i.c.v.) routes. Following i.t. injection of cell-penetrant RNPs, we observed edited glial cells and

neurons in the cortex and striatum of one hemisphere, but no editing within the spinal cord (Figure S3A). Following i.c.v. injection of Cas9 RNPs in neonatal p0 mice, we observed tdTomato$^+$ cells in the subventricular zone and white matter, including glial cells and neural stem/progenitor cells expressing Ki67 and DCX evaluated 3 weeks after delivery (Figures S3B and S3C). Editing post-i.c.v. injection in adult mice was restricted to the cells within the lateral ventricles, choroid plexus, subventricular zone, and hippocampus in a subset of mice (Figures S3D and S3E). The total number of edited cells with RNP delivery into the CSF was lower than with direct intraparenchymal injection (Figure S3F).

Therefore, we sought to further improve upon intraparenchymal injections using a CED system, which generates a high-pressure gradient to aid in biodistribution of macromolecules in the brain. CED has been used to increase the spread of AAV in the brains of large animal models and humans by infusing relatively high injection volumes at high rates.[33,34] In addition, we tested two needle designs to enable CED with Cas9-RNPs. We found that the CED enabled robust editing in the mouse striatum (Figure S4) and the step-cannula reduced reflux of RNP from the needle-injection track, as reported previously[35] (Figure 1D). Furthermore, tdTomato$^+$ neurons edited by Cas9-RNPs within the striatum were observed to extend along the basal ganglia circuit into the globus pallidus and substantia nigra along the anterior-posterior axis (Figure 1E).

CED of Cas9 RNPs and AAVs mediates robust editing in the mouse striatum

Using bilateral CED injections into the striatum, we compared edited tissue volume with the 4x-SpyCas9-2x RNP, 4x-SauCas9-2x RNP, and AAV9-SauCas9-sgRNA in adult Ai9 mice at 3 weeks post-injection. Despite performing well *in vitro*, 4x-SauCas9-2x RNPs underperformed *in vivo* when tested at two different doses and additional NLS configurations (Figure S5). Therefore, we performed our primary comparison with two orthologous systems: 4x-SpyCas9-2x RNP (hereafter referred to as Cas9-RNP) and AAV9-SauCas9-sgRNA (hereafter referred to as Cas9-AAV, which serves as a positive control, Figure 1F).

First, we tested Cas9-AAV injection with CED at two doses, 3×10^8 and 3×10^9 vg/μL (1.5×10^9 to 1.5×10^{10} vg/hemisphere),[36] and proceeded with the higher dose for subsequent studies *in vivo* (Figures S6A and S6B). We also tested several doses of Cas9-RNP ranging from 10 to 100 μM (50–500 pmol/hemisphere). Interestingly, there was no significant difference in editing when delivering RNPs in this concentration range (Figures 1H and S6C). We chose the 25-μM RNP concentration (4.15 mg/mL or approximately 1.75 mg/kg Cas9) group for further study as it had the highest maximal editing rate. Above 25μM in the RNP group, we observed a decrease in NeuN staining and an increase in GFAP staining out to 90 days in the Cas9-RNP group, suggesting dose-limiting effects (Figure 1G).

At both 21 and 90 days post-injection, the Cas9-AAV group outperformed the Cas9-RNP group when quantifying total edited striatal volume (n = 8 at 21 days, n = 4 at 90 days, p < 0.05, Figure 1I).
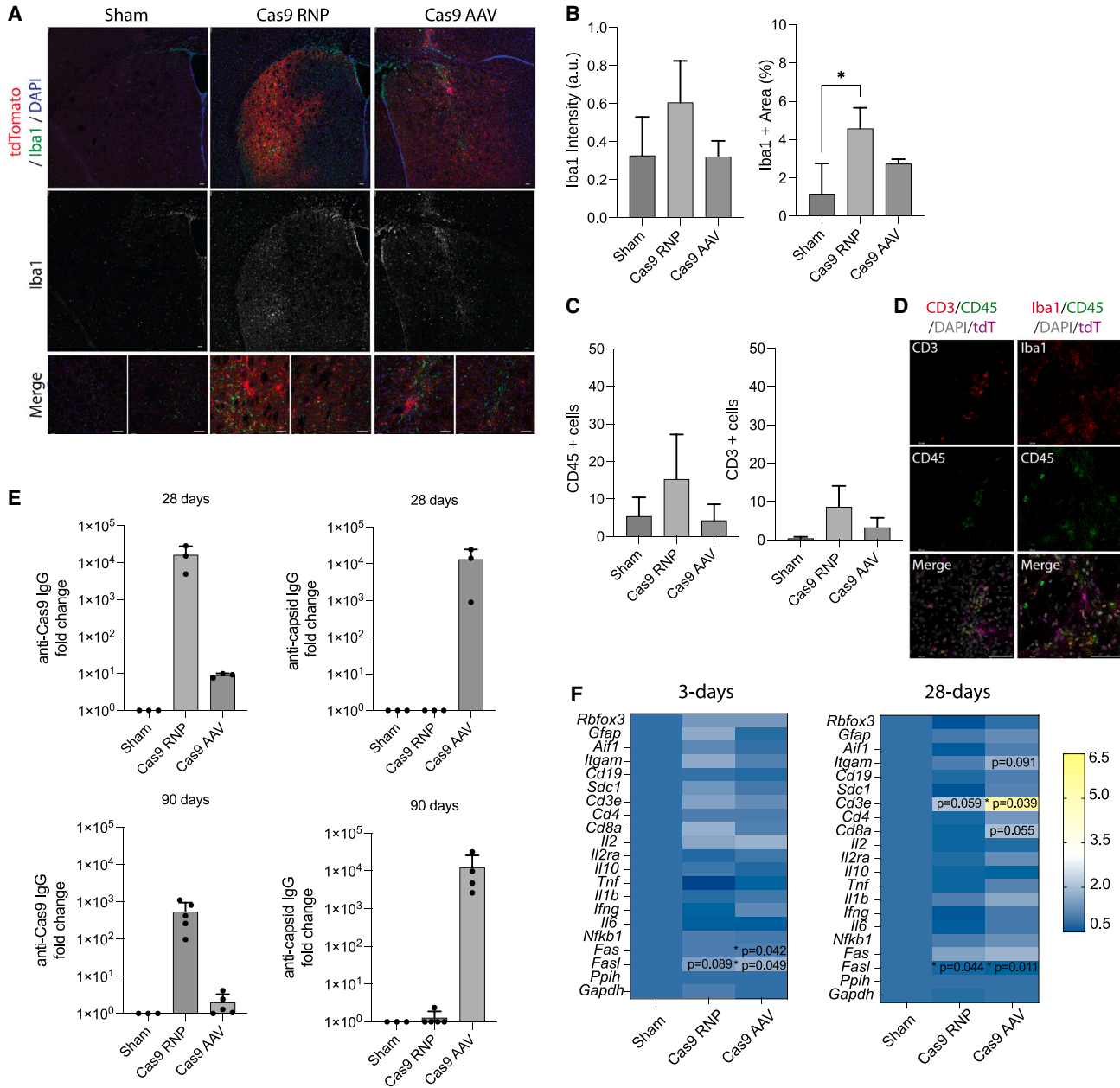
Figure 2. Immune response following *in vivo* editing with viral and non-viral Cas9 delivery strategies

(A) Representative immunostaining of Iba1 (microglia, green) with tdTomato and DAPI using confocal microscopy. Scale bar, 50 μm. (B) Quantification of Iba1$^+$ staining intensity and percent area (n = 4–6 technical replicates, one-way ANOVA, *p < 0.05). (C) Quantification of CD45$^+$ and CD3$^+$ cells per image (n = 3–6 replicates, one-way ANOVA, ns). (D) Representative images of CD45, CD3, and Iba1 showing co-expression of CD45 (green) with both Iba1 (microglia, red) and CD3 (T cells, red) cells and differential cell morphology. Merged images include DAPI (gray) and tdTomato (magenta). Scale bars, 50 μm. (E) Quantification of IgG antibodies against Cas9 or AAV capsid proteins measured 28 and 90 days after bilateral intrastriatal injections by ELISA (n = 3–5 biological replicates). (F) Heatmap summarizing qRT-PCR results of gene expression from homogenized brain tissue near the injection site (striatum and cortex) at two time points. *Ppih* was used as a housekeeping control for delta-delta Ct analysis and compared with the sham group using the QIAGEN analysis portal (n = 4, *p < 0.05).

The volume of edited cells was relatively stable in the Cas9-AAV group between 21 and 90 days at approximately 47% ± 3% (covering approximately 13.4 mm^3 of striatum), while the Cas9-RNP group had editing levels of 22% ± 3% (approximately 6.2 mm^3 of striatum) between 21 and 90 days (increased from previous report of editing 1.5 mm^3 striatal volume[19]). Edited cells were observed further along

the rostral-caudal axis in the Cas9-AAV group (-2.12–2.5 mm relative to bregma), demonstrating better diffusion of the editor away from the injection site (Figures S6E and S6F).

Since large deletions in the tdTomato locus make on-target editing difficult to assess using short-read next-generation sequencing (NGS), we developed an NHEJ droplet digital PCR (ddPCR) assay to measure drop-off of HEX-labeled probes over the cut sites in relation to distal reference FAM-labeled probes. Genomic DNA was isolated from 2-mm-thick sections of each injected hemisphere, covering multiple brain sub-structures. Loss of the HEX probe reached 2% ± 1% in the Cas9-RNP group and 15% ± 10% in the Cas9-AAV group, indicating edited alleles, when measured at 28 days (Figure S7).

We also quantified the percentage of edited NeuN$^+$ neurons within the tdTomato$^+$ region of interest (ROI) per hemisphere between Cas9-AAV and Cas9-RNP at the 21-day time point. We found that Cas9-RNP edited significantly more NeuN$^+$ neurons per ROI (36% ± 10%) compared with Cas9-AAV (20% ± 2%) (Figure 1J, n = 6–8 injections, p < 0.05). Within the ROI, neurons were the most frequently edited cell type in both groups, including DARPP-32$^+$ medium spiny neurons (Figure S8). In addition, editing of ALDH1L1$^+$ and OLIG2$^+$ glial cells was noted in both groups (approximately 2% of edited cells within the ROI in the Cas9-RNP group and 8% of cells in the Cas9-AAV group). Therefore, Cas9-RNPs were able to edit comparable numbers of neurons and glia as Cas9-AAVs within a given area of striatal tissue.

Comparison of local and peripheral immune response between Cas9 RNPs and AAVs in the Ai9 reporter mouse

We next examined the local and peripheral immune response following delivery of Cas9 RNPs and AAVs into the brain. Using immunofluorescent staining for Iba1 (Figure 2A), we observed a significant increase in percent Iba1$^+$ area in the 25-μM Cas9-RNP group from sham-treated animals (Figure 2B, n = 6 replicates, p < 0.05). Staining for CD45 showed co-expression on Iba1$^+$ microglia and CD3$^+$ T cells, which were slightly increased in the 25 μM Cas9-RNP group compared with the sham and Cas9-AAV, but not significantly different, at 3 weeks post-injection (Figures 2C and 2D, n = 6–12 replicates).

In addition to the immune response at the local site of injection, circulating IgG antibodies were measured at 28 and 90 days post-injection. We found that sham-treated animals had no pre-existing antibodies to SpyCas9, SauCas9, or AAV9 capsids. At 28 days after striatal injection, there was a 1.6e4-fold increase in anti-SpyCas9 IgG in the 25-μM Cas9-RNP group, a 1.3e4-fold increase in anti-AAV9 capsid IgG in the Cas9-AAV group, and an 8.9e1-fold increase in anti-SauCas9 IgG in the Cas9-AAV group (i.e., humoral response against expressed transgene) (Figure 2E, n = 3–5 biological replicates). No cross-reactivity was observed between ortholog RNPs, as described previously,[11] nor were any anti-AAV capsid antibodies detected in the RNP group. At 90 days, the levels of IgG fell to a 5.4e2-fold increase in the 25-μM Cas9 RNP group and 1.2e4-fold increase in the Cas9 AAV group from

the sham controls, demonstrating greater maintenance of systemic antibodies against the capsid in the AAV group.

The cellular and humoral immune response to Cas9 RNPs was dose dependent and a significant increase in CD45$^+$ cells was observed at the 100-μM RNP dose compared with sham, Cas9-AAV, and Cas9-RNP at 25 μM (Figures S9A–S9D). Cas9-reactive cells were also identified in the spleen by interferon-gamma (IFN-γ) enzyme-linked immunospot (ELISpot) assay (Figure S9E) at both 25- and 100-μM doses of Cas9-RNPs, but not in sham-treated animals.

Since the mice had no pre-existing antibodies to SpyCas9, we tested how the immune response would differ in the RNP group by first exposing the mice to a single subcutaneous injection of 4x-SpyCas9-2x protein with adjuvant (AddaVax) 4 weeks before stereotaxic surgery with Cas9-RNPs. We found that pre-exposing the mice to Cas9 and adjuvant had a synergistic effect on both serum IgG and activation of IFN-γ^+ cells in the spleen (Figures S9F–S9I). Mice that received surgery maintained tdTomato$^+$ cells in the brain to the measured time point. Additional studies using this immunization strategy may help to further characterize the immune response to Cas9-RNPs.

Finally, we measured gene expression changes near the injection site in mice that received Cas9-RNP and AAV at 3 and 28 days post-injection using qRT-PCR. At 3 days, the Cas9-AAV group had a modest but significant increase in Fas (1.19-fold) and Fasl (1.85-fold) compared with the sham group (Figure 2F, n = 4 replicates, p < 0.05). At 28 days post-injection, both Cas9-RNP and -AAV had a significant increase in Fas (1.61- and 1.89-fold, respectively). In addition, the Cas9-AAV group had a significant increase in Cd3e gene expression (5.45-fold, p = 0.039), closely followed by Cd8a (2.06-fold, p = 0.055), while Cas9-RNP had a slight but non-significant increase in Cd3e (2.15-fold, ns, p = 0.059) compared with the sham group.

There were no detectable off-target editing events at 1 and 4 months post-injection in any of the experimental groups at the evaluated sites (Figures S10A–S10C). In the Cas9-AAV group, the Cas9 transgene was expressed in the brain out to 4 months, the last tested time point, as expected (Figure S10D). In addition, few genes were differentially expressed between the groups at 4 months, except for Fas (1.54-fold, p < 0.05), which was significantly elevated in the Cas9-AAV group compared with the sham (Figures S10E and S10F). We used long-read sequencing to examine whether any fragments of the viral genome had been integrated near the cut site in the tdTomato locus, as reported previously.[37–40] We also observed partial integrations of viral fragments in our amplicon, although our in vivo editing rates and sequencing depth were relatively low (Figure S11).

Overall, delivery of Cas9 by either AAV or RNP resulted in activation of immune responses in the brain and periphery, although with generally small effect sizes compared with sham-injected mice. The increased Iba1$^+$ cells near tdTomato$^+$ cells in the striatum of the 25-μM Cas9-RNP group raised the question of whether the response
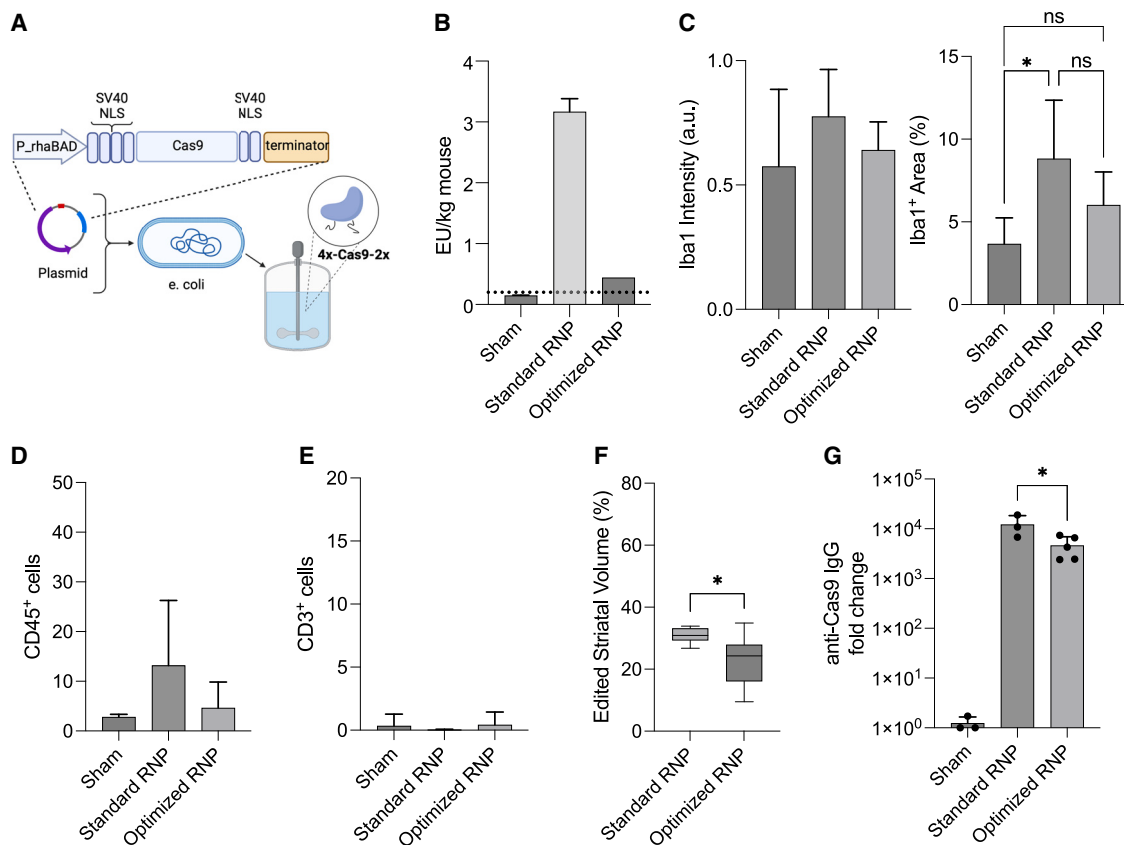
Figure 3. Optimized, low endotoxin RNP formulation reduces local immune response

(A) Schematic of manufacturing scale-up to produce industrial ultra-low endotoxin 4x-SpyCas9-2x protein using a tag-free expression and purification system. (B) Endotoxin levels calculated on a per mouse basis between the standard (laboratory 4x-SpyCas9-2x with sg298 2018) and optimized (industrial 4x-SpyCas9-2x protein with sg298 2022) RNP formulations at 25 μM measured by LAL assay. Dotted line indicates FDA recommendation of 0.2 EU/kg/h for drug products administered intrathecally in humans. (C) Quantification of Iba1$^+$ staining intensity and percent area (n = 6–10, one-way ANOVA, *p < 0.05). (D) Quantification of CD45$^+$ and (E) CD3$^+$ cells per image (n = 6–10, one-way ANOVA, ns). (F) Percent volume of edited striatal tissue for Cas9 RNPs injected at 25 μM (n = 6–10 injections). (G) Quantification of IgG antibodies against Cas9 or AAV capsid proteins measured 21 days after bilateral intrastriatal injections by ELISA (n = 3–5 biological replicates).

was due to Cas9 itself or impurities within the protein product. We hypothesized that the local immune response may be due to endotoxins from *E. coli* in the RNP complexes.

Production and testing of ultra-low endotoxin 4x-SpyCas9-2x protein

To examine the impact of endotoxin on the immune response to RNPs, we partnered with a commercial producer of Cas9 protein and were able to significantly scale-up manufacturing to produce a large quantity of ultra-low endotoxin 4x-SpyCas9-2x protein using an industrial tag-free expression and purification system (Figure 3A).

Using the limulus amebocyte lysate (LAL) assay, we measured an endotoxin concentration of 0.035 EU/mg in the industrial-produced protein compared with 0.2 EU/mg in the lab-produced protein (Figure S12). Interestingly, using the same assay, we found that guide RNA could be an unexpected source of endotoxin contamination.

Endotoxin was present in at least three unopened vials of lyophilized RNA that had been stored at −80°C from a 2018 lot, but not in a more recently purchased lot from the same vendor when resuspended simultaneously (Figures S12A–S12C). To rule out false positives due to reaction of LAL with beta-glucans, we performed the recombinant factor C (rFC) assay. We measured a similar level of endotoxins in the guides between the LAL and rFC assays, demonstrating the positive signal was from contamination with endotoxin and not beta-glucans (Figures S12D and S12E). Furthermore, the amount of endotoxin increased with dose of RNP and was substantially reduced with the new guide and protein, as expected (Figures S12F and S12G).

To measure the physiological impact of endotoxin in our samples, we used HEK293 cells that were engineered to produce secreted embryonic alkaline phosphatase (SEAP) downstream of NF-κB activation resulting from human Toll-like receptor 4 (hTLR4) stimulation with endotoxin/lipopolysaccharide (LPS) (Figures S13A–S13C). The

lab-produced protein stimulated NF-κB in HEK293 cells significantly greater than the industrial produced protein (Figure S13D, p < 0.01, unpaired t test). Treatment with the industrially produced protein led to similar levels of SEAP between hTLR4 cells and the parental cell line (Null2), demonstrating that most of the NF-κB stimulation was downstream of other pattern-recognition receptors (such as TLR3, TLR5, or nucleotide-binding oligomerization domain-containing protein 1 activation) and not due to LPS signaling through hTLR4. When combined with sg298 from the 2018 or 2022 lots, absorbance levels of SEAP further increased in RNP complexes made with lab-produced protein, while the industrial protein with either guide did not induce a response (Figure S13E). Furthermore, guide RNA alone did not stimulate NF-κB in HEK293 cells (Figure S13F).

Finally, we measured endotoxins in the "optimized" formulation of RNPs, comprised of the industrially produced 4x-SpyCas9-2x protein and 2022 lot of sgRNA, using the LAL assay. Estimating delivery of 10 μL per mouse, the endotoxin burden was 0.44 EU/kg when RNPs were formulated at 25 μM. These data suggest that RNPs could be delivered below the 0.2-EU/kg FDA threshold for i.t. delivery[41] when formulated at 10 μM without significant loss of editing (Figures 3B and 1H).

Optimized RNP formulation reduces immune response

We performed CED bilateral intrastriatal injections to test if reducing endotoxins would improve the host immune response to RNPs *in vivo*. In this experiment, we compared the optimized RNP formulation (industrially produced 4x-SpyCas9-2x NLS protein with sg298 2022) to the standard formulation used in Figures 1 and 2 (laboratory produced 4x-SpyCas9-2x NLS protein with sg298 2018) at 25 μM. The standard RNP induced a significant increase in Iba1$^+$ area, consistent with our previous measurements (Figures 3C and 1A); however, the optimized Cas9-RNP formulation did not induce microglial activation. In addition, there was no increase in CD45$^+$ and CD3$^+$ cells from the sham in the optimized RNP group (Figure 3D). Of note, the standard RNP edited an average of 31% ± 3% striatal volume (greater than values reported in Figure 1, possibly due to differences between protein lots or injections), while the optimized RNP edited an average of 23% ± 8% striatal volume (Figure 3F). When tested *in vitro*, the optimized RNP performed slightly better at direct delivery than nucleofection compared with the standard formulation, which could explain in part the differences *in vivo* (Figure S14A). Interestingly, the standard RNP also led to significantly greater anti-Cas9 IgG responses at 3 weeks post-injection, possibly due to endotoxin boosting the adaptive immune response (Figure 3G). Taken together, we found that reducing endotoxins in both the guide RNA and protein components of the RNP leads to a reduced innate immune response, comparable with the sham, while maintaining high on-target editing. Furthermore, cell-penetrant Cas9 proteins are amenable to fast and cost-effective manufacturing of large quantities suitable for *in vivo* experiments.

In conclusion, our results establish complementary genome editing and immunogenicity outcomes between the two tested Cas9 delivery strategies (Figure S14B). To enable high levels of editing in neurons within a localized brain region, minimizing adaptive immune responses, and timely and affordable manufacturing scale-up, the RNP offers an effective alternative delivery system to viral vectors.

DISCUSSION

In this study, we demonstrate that cell-penetrant Cas9 RNPs edit a significant volume of the mouse striatum using CED. Furthermore, the 4x-NLS modification enables self-delivery of multiple Cas9 orthologs to neuronal cells from both mouse and human species. We also show that Cas9 RNPs have dose-dependent effects on the immune response, which can be mitigated by using ultra-low endotoxin protein produced in an industrial non-GMP setting. These experiments are informative for the design of future therapeutic applications of Cas9 RNP editors in mice and larger animal models.

Several studies have reported non-viral delivery of Cas9 into the mouse brain. The "CRISPR-Gold" Cas9 nanoparticle delivery system induced 14% edited glial cells near the injection site, sufficient to reduce repetitive behaviors in a mouse model of fragile X syndrome.[42] In addition, incubating RNPs with R7L10, an arginine- and leucine-rich cationic peptide, induced 45% indels in the CA3 region of the hippocampus, leading to behavioral improvements in an Alzheimer's disease mouse model.[43] Efficient editing of DARPP-32 medium spiny neurons in the striatum was achieved here and in recent work by others using RNPs packaged in biodegradable PEGylated nanocapsules.[44] Interestingly the PEGylated nanocapsules have a neutral charge, while 4x-Cas9-2x NLS RNPs have a net-positive charge, suggesting that the mechanism of entry may differ between the two strategies. Systemic delivery of genome editors with glucose-conjugated silica nanoparticles and AAV9 can also lead to modest levels of editing in the brain, sufficient for therapeutic benefit.[45,46] Despite the need for direct injection, the simplicity of the 4x-Cas9-2x RNP is ideal from a manufacturing perspective compared with other formulations. In the future, the RNP injection buffer could be further supplemented with polymers, such as polyethylene glycol,[47,48] to potentially improve distribution in the brain.

Several studies show correlation between editing at the tdTomato locus and subsequent editing at endogenous sites[42,45,49] and future work will focus on genome editing at therapeutically relevant targets. It is important to note that expression of the tdTomato protein in the Ai9 mouse model underreports the actual genome editing efficiency, as double-strand breaks that result in indels and small deletions are not sufficient to turn on the reporter.[19] We sought to further resolve editing outcomes with a ddPCR assay, since the tdTomato locus is too large for Illumina-based NGS. In the ddPCR probe drop-off assay we detected approximately a 6-fold difference in editing with AAV compared with RNP (approximately 15% vs. 2.5% indels), whereas our immunofluorescent measurement showed a 2-fold increase. We speculate that the difference in reported editing efficiency between the two assays is based on the sampling methodology. The image analysis workflow quantified the volume of striatal tissue containing edited cells (Figure 1I), where 20%–36% of neurons were edited within 25%–50% of the striatum (Figure 1J). Therefore, the image quantification reflects the maximal distribution of edited cells in the striatum. The

ddPCR assay utilized genomic DNA (gDNA) from 2-mm-thick tissues dissected from the expected injection site including the striatum, as well as the cortex and corpus callosum, which likely favors editing events in the Cas9-AAV group due to its enhanced diffusion through the brain. While dose escalating the RNP did not improve editing levels, suggesting a saturating dose was already achieved as measured by image quantification, editing at different doses was not assessed using ddPCR. Furthermore, increasing the dose of Cas9-AAV may have further increased editing levels. Studies suggest that correcting pathological mutations in 20%–30% of striatal neurons expressing mutant huntingtin protein is sufficient to significantly improve the disease pathology, therefore even modest editing levels in the striatum could enable therapeutic benefit.[50] Ultimately, behavioral assays are needed to further determine therapeutic benefit of the RNP approach in a disease-relevant model.

We hypothesized that cell-penetrant Cas9-RNPs would be less immunogenic than Cas9-AAVs due to their transient expression. As the dose of 4x-SpyCas9-2x RNPs increased from 25 to 100 μM, there was an increase in CD45$^+$ and GFAP$^+$ cells, and a decrease in NeuN$^+$ cells. As such, subsequent experiments were performed at 25 μM, which was well tolerated and resulted in similar levels of editing as the higher dose. The 25-μM Cas9-RNP dose led to lower levels of vehicle-specific antibodies by 90 days post-injection compared with Cas9-AAVs and did not upregulate gene signatures of T cells at 28 days as measured by qRT-PCR, supporting our hypothesis. By 90 days, the levels of anti-Cas9 antibodies in the Cas9-AAV group were only elevated in three out of five mice, demonstrating that the kinetics of Cas9 antibody persistence may be similar between RNPs and AAVs, despite stable, intracellular Cas9 expression. Reducing endotoxin in both the Cas9 protein and guide RNA prevented microglial reactions and reduced humoral responses at 21 days.

In the Cas9-AAV group, few immune cells (CD45, Iba1, or CD3) were observed in the striatum by immunostaining; however, *CD3e* gene expression was significantly upregulated in explanted tissue, closely followed by an increase in *CD8a*. This finding could indicate accumulation of cytotoxic T cells trafficking into the parenchyma from the blood vessels or CSF. In addition, no changes in NeuN, GFAP, and CD45 expression were observed in the Cas9-AAV group out to 4 months, demonstrating that the AAV delivery strategy was well tolerated overall in naive mice. A study by Li et al. found that mice immunized against SauCas9 with Freund's adjuvant 1 week before intravenous delivery of AAV8-SauCas9-sgRNA resulted in accumulation of cytotoxic T cells in the liver and subsequent removal of edited hepatocytes.[12] Therefore, the host immune response to Cas9-AAV in mice with pre-existing immunity would likely be different than what we observed in naive mice. In the Cas9-RNP group, we found that pre-exposing mice to SpyCas9 protein with AddaVax adjuvant 4 weeks before stereotaxic surgery synergistically increased systemic adaptive immune responses. Further studies are needed to assess the immune response to Cas9-AAV and RNP in models with pre-existing immunity, but how well these immunized mouse models recapitulate pre-existing immunity in humans is not clear. Further-

more, breakdown of the BBB in the context of neurodegenerative disease or strong expression of the tdTomato fluorescent reporter could also impact the host immune response.[51,52]

In this study, we used a strong CMV-promoter to drive expression of SauCas9 from the AAV, which allowed us to assess all subsets of edited cells in the striatum, in comparison with the RNP, which is not inherently designed to be neuron specific. Although the SauCas9 transgene was still expressed 4 months post-delivery, editing at predicted off-target sites was not detected. Further work to experimentally determine guide-specific off-target sites, such as Guide-Seq[53] or Circle-Seq,[54] was not performed. To prevent potential genotoxic side effects due to long-term Cas9 expression, we recommend applying additional safeguards, such as AAV self-inactivation strategies, and neuron-specific promoters, such as human synapsin 1, to increase cell specificity.[55–57] While self-inactivating AAVs may improve safety, they may not be sufficient to prevent integration of the viral genome at the Cas9 cut site, which has been reported.[37–40] Strategies to mitigate the host response to genome editors, including immunosuppressants and screening for pre-existing immunity before dosing, should also be implemented when translating *in vivo* editing to humans.[58]

While SpyCas9 is generally the most efficacious and widely used type II CRISPR protein to date, it is too large to be packaged in a single AAV with sgRNA. Therefore, in this study, we used AAV-CMV-SauCas9-U6-sgRNA as a positive control to benchmark delivery of RNPs, as similar AAV constructs have been used extensively in the literature and in clinical trials.[12,23,24,59] *In vivo* delivery of 4x-Sau-Cas9-2x RNP did not lead to significant editing; thus, most comparisons were performed between two orthologous genome editors and delivery systems with different NLS configurations, which may impact the interpretation of this work. *In vivo* editing with 4x-Sau-Cas9-2x RNP was possibly hindered by the reduced thermostability of the protein, as reported previously.[60] Employing Cas9 RNPs from a more thermostable organism could be advantageous in the future. Since RNPs are not restricted by cargo packaging, one advantage of the cell-penetrant RNP technology is the ability to use SpyCas9 for future therapeutic applications in the brain.

In conclusion, the cell-penetrant 4x-Cas9-2x NLS fusion protein enables simple and effective delivery of Cas9 RNPs into neuronal cells *in vitro* and *in vivo*. To our knowledge, this study is the first to examine the host immune response to Cas9 in the brain, benchmark an RNP delivery strategy against the gold standard for gene delivery in the CNS, and demonstrate feasibility of large-scale manufacturing of cell-penetrant Cas9 protein. Given that Cas9-RNPs excel at editing high levels of neurons within a localized region of the brain, this is a promising modality to characterize therapeutic benefit in disease models in the future.

MATERIALS AND METHODS
Plasmid construction
Guide spacer sequences were cloned into a plasmid encoding SauCas9 (pSTX8,pKLT7.1_SaCas9prot_SaCas9guide) as described previously.

In brief, oligonucleotides encoding the spacers were custom synthesized (Integrated DNA Technologies [IDT], Coralville, IA) and phosphorylated by T4 polynucleotide kinase (New England Biolabs, Ipswich, MA) for 30 min at 37°C. Oligonucleotides were annealed for 5 min at 95°C, cooled to room temperature, and ligated into the BsmBI restriction sites of the plasmid. The following 23-nt spacer sequences were cloned into the plasmid (spo 1: TGGTATGGCTGATT ATGATCCTC; spo2: TCCCCCTGAACCTGAAACATAAA; spo3: GATGAGTTTGGACAAACCACAAC; spo4: TCCAGACATGGATA CATTGATAA; spo5: CTCATCAATGTATCTTATCATGT), and plasmids were used for editing in mouse NPCs in vitro. The best performing SauCas9 spacer (spo4: TCCAGACATGATAAGATACATTG) was then cloned into an AAV2 backbone plasmid. pX601-AAV-CMV:: NLS-SaCas9-NLS-3xHA-bGHpA; U6::BsaI-sgRNA was a gift from Feng Zhang (Addgene plasmid no. 61591; http://n2t.net/add gene:61591; RRID:Addgene_61591). In brief, the plasmid was digested using BbsI and a pair of annealed oligos were cloned into the guide RNA destination site by Golden Gate assembly. For SpyCas9, the sg298 spacer sequence (5′ AAGTAAAACCTCTACAAATG) was used to target td Tomato.[19] Correct construction of all plasmids was verified by Sanger sequencing (UC Berkeley DNA Sequencing Facility).

Recombinant AAV production

The custom AAV9-CMV-61591-HA-Bgh vectors were produced at Virovek (Hayward, CA) in insect Sf9 cells by dual infection with rBV-inCap9-inRep-hr2 and rBV-CMV-61591-HA-Bgh. The AAV9-CMV-GFP vectors were produced by dual infection with rBVinCap9-inRep-hr2 and rBV-CMV-GFP. The vectors were purified through two rounds of cesium chloride (CsCl) ultracentrifugation. The CsCl was removed through buffer exchange with two PD-10 desalting columns. Viral titer (approximately 2e-13 vg/mL) and purity were confirmed by NanoDrop spectrophotometer, real-time PCR, and SDS-PAGE protein gel analysis. The vectors were passed through 0.2-μm sterilized filters, tested for endotoxins (<0.6 EU/ mL), as well as baculovirus and Sf9 DNA contamination (not detected).

Purification of low endotoxin proteins in a laboratory setting

Protein expression and purification was performed in the QB3 Macrolab at UC Berkeley using a custom low endotoxin workflow. In brief, the plasmid, 4xNLS-pMJ915v2 (Addgene plasmid no. 88917; http://n2t.net/addgene:88917; RRID:Addgene_88917), was transformed into E. coli Rosetta2(DE3)pLysS cells (Novagen) and an overnight culture was used to inoculate 1-L flasks (12–24 L total per batch). Cells were grown for approximately 3 h at 37°C then cooled to 16°C. At optical density (OD) of 0.8–0.9, cells were induced and harvested after 16–18 h growth. Cells were lysed by homogenization in a buffer containing 1 mM $MgCl_2$ and benzonase (1:1,000) to help reduce viscosity and centrifuged to remove insoluble material. Purification by Ni affinity (10 mL Ni resin for every 6 L cell lysate) was performed, and the bound protein was washed with 10 column volumes of buffer containing 0.1% Triton X-114 at 4°C to reduce endotoxins. Tag removal with TEV protease (1:100) was performed overnight at 4°C, then heparin affinity was used to concentrate each batch of pro-

tein, which was then flash frozen and stored at −80°C. A Sephacryl S300 size-exclusion column and flow path were sanitized with 0.5 M NaOH overnight, then washed with up to 3 column volumes of buffer to rinse and equilibrate the system. Frozen samples were thawed, combined, and adjusted to 4.5 mL, and the protocol was performed for size exclusion. Samples were refrigerated overnight. Sanitation and size exclusion were repeated the next day to further improve purity. Peak fractions were pooled, concentrated to 40 μM, aliquoted at 50 μL, flash frozen in liquid nitrogen, and stored at −80°C in sterile, endotoxin-free buffer 1 (25 mM NaP [pH 7.25], 300 mM NaCl, 200 mM trehalose [Sigma-Aldrich, St. Louis, MO, no. T5251]). The final average protein yield was 1 mg per 1 L cells. Plasmids for 2xNLS-SauCas9-2xNLS, 3xNLS-SauCas9-2xNLS, and 4xNLS-SauCas9-2xNLS were created by deletion mutagenesis using the existing 4xNLS-SpyCas9-2xNLS construct as a template. Correct construction of all plasmids was verified by Sanger sequencing (UC Berkeley DNA Sequencing Facility).

Purification of ultra-low endotoxin proteins in an industrial setting

4x-SpyCas9-2x NLS protein was manufactured according to Aldevron proprietary workflows for expression and purification of gene editing nucleases. In brief, the gene for 4x-SpyCas9-2x NLS was synthesized (ATUM, Sunnyvale, CA) and cloned into a pD881 expression vector (ATUM). Expression-ready plasmid DNA was transformed into E. coli BL21(DE3) (New England Biolabs) culture in animal-free TB medium. At the appropriate OD_{600}, expression was induced with 2.0% (w/v) Rhamnose and growth culture was harvested by centrifugation. Cells were lysed via dual-pass high-pressure homogenization and clarified via centrifugation. The clarified lysate was purified via multi-step chromatography using standard/commercially available resins. In the final chromatography step, the product is eluted via step elution and pooled to maximize final protein purity and minimize endotoxin. Product was dialyzed into the final formulation buffer, underwent three exchanges of buffer, and was pooled into a sterile vessel for final filtration and dispensing. Product was evaluated for key quality attributes including endotoxin via PTS Endosafe assay (Charles River, Cambridge, MA).

Quantification of endotoxins in Cas9 RNPs

Proteins, guide RNAs, and RNP complexes were subjected to several assays to quantify endotoxin burden according to the manufacturer's instructions. Assays were performed with autoclaved or certified pyrogen-free plasticware and endotoxin (ET)-free water. The plate-reader-based LAL assay was performed with the Endosafe Endochrome-K kit (Charles River, no. R1708K), where a control standard endotoxin (CSE) was diluted from 5 to 0.005 EU/mL. Samples were diluted 1:100 and plated in triplicate. An equal volume of LAL was added to each well. A Tecan Spark plate reader (Tecan, Männendorf, Switzerland, no. 30086376) with SparkControl magellan v.2.2 software was used at 37°C to read absorbance at 405 nm every 30 s for at least 80 cycles. Time at which absorbance crossed an OD of 0.1 was recorded and used to determine endotoxin levels.

The cartridge-based LAL assay was performed using an Endosafe nexgen-PTS machine with R&D cartridges as recommended (Charles River, cat. no. PTS2005, 0.05 EU/mL sensitivity). In brief, samples were diluted 1:50 in a large volume of ET-free water, vortexed, and 25 μL was loaded into each of the four lanes of the cartridge, where two lanes contain CSE spike-in to calculate efficiency of the assay, which is valid from 50% to 200% recovery. The final valid ET value was recorded from the duplicate measurement from a single cartridge.

The PyroGene Recombinant Factor C Endpoint Fluorescent Assay (Lonza, Walkersville, MD, cat. no. 50-658U) was performed as recommended. Kit-supplied CSE was diluted from 5 to 0.005 EU/mL and samples were diluted 1:100 in ET-free water and added to a plate in triplicate. The plate was heated at 37°C for 10 min, then an equal volume of working reagent was added to each well. Fluorescence was read immediately at time 0 and after incubating for 60 min. Relative fluorescence units (RFUs) of the ET-free water only blank wells were subtracted from all measurements, then delta RFUs between the two time points was calculated, and a linear regression was applied to the standard curve to calculate EUs in the samples. Fluorescence measurements were performed on a Cytation5 with Gen 5 3.04 software (BioTek, Winooski, VT).

HEK-Blue cells (hTLR4 and Null2) were purchased from Invivogen (San Diego, CA) and were grown under BSL2 conditions (37°C with 5% CO_2) to measure SEAP production downstream of NF-κB activation following treatment with Cas9 proteins, guide RNAs, and RNPs *in vitro* as recommended. Cells were grown in T-75 flasks with supplied antibiotic selection markers and passaged at 70% confluency. Cells were detached with gentle scraping in $1\times$ PBS, centrifuged, counted, and plated for experiments in freshly prepared HEK-Blue Detection Medium at approximately 32,000 cells per well in a 96-well plate. Cell suspension (180 μL) was plated directly into 20 μL of diluted CSE (5–0.078 ng) or samples (diluted to 10 μM) and incubated overnight at 37°C. Absorbance was read at 620 nm in a Tecan Spark plate reader.

NPC line creation and culture
NPCs were isolated from Ai9-tdTomato homozygous mouse embryos (day 13.5) by microdissection of cortical tissues into Hibernate E (#HECA, BrainBits LLC, Springfield, IL) and processing with the Neural Dissociation Kit with papain (Miltenyi, Bergisch Gladbach, Germany, no. 130-092-628) according to the manufacturer's instructions. Single cells grew into non-adherent neurospheres, which were maintained in culture medium (DMEM/F12 [Thermo Fisher Scientific, Waltham, MA, no. 10565-018], B-27 supplement [no. 12587-010], N-2 supplement [no. 17502-048], MEM non-essential amino acids [no. 11140-050], 10 mM HEPES [no. 15630-080], 1,000× 2-mercaptoethanol [no. 21985-023], 100× Pen/Strep [no. 15140-122]) supplemented with growth factors (FGF-basic [BioLegend, no. 579606] and EGF [Thermo Fisher Scientific, no. PHG0311]) to a final concentration of 20 ng/mL in medium. Neurospheres were passaged every 6 days using the Neural Dissociation Kit to approxi-

mately 1.5 million cells per 10-cm dish and growth factors were refreshed every 3 days. Cells were authenticated by immunofluorescent staining for Nestin and GFAP, routinely tested for mycoplasma, and were used for experiments between passages 2 and 20. Dissociated cells were grown in monolayers in 96-well plates pre-coated with poly-DL-ornithine (Sigma-Aldrich, no. P8638), laminin (Sigma-Aldrich, no. 11243217001), and fibronectin (Sigma-Aldrich, no. F4759) ("PLF") for direct delivery and nucleofection experiments at approximately 30,000 cells per well.

Human iPSC differentiation into NPCs and culture
MSC-iPSC1 cells were a generous gift from Boston Children's Hospital. iPSCs were differentiated into NPCs based on dual SMAD inhibition as described previously. In brief, iPSCs were plated onto Matrigel in the presence of 10 μM Y-27632 (Sigma, no. Y0503) at a density of 200,000 cells/cm^2. The next day (day 0) medium was changed to KSR medium (Knockout DMEM [Thermo Fisher Scientific, no. 10829018], 15% Knockout serum replacement [Thermo Fisher Scientific, no. 10828010], L-glutamine [1 mM], 1% MEM non-essential amino acids, and 0.1 mM β-mercaptoethanol). Medium was changed daily during differentiation and gradually changed from KSR medium to N2/B27 medium (Neurobasal medium [Thermo Fisher Scientific, no. 21103049], GlutaMAX supplement [Thermo Fisher Scientific, no. 35050061], N-2 supplement [Thermo Fisher Scientific, no. 17502048], and B-27 supplement [Thermo Fisher Scientific, no. 17504044]) by increasing N2/B27 medium to 1/3 on day 4, 2/3 on day 6, and full N2/B27 medium on day 8. For the first 12 days of differentiation, the medium was supplemented with 100 nM LDN193189 (Sigma, no. SML0559) and 10 μM SB431542 (Tocris Bioscience, Bristol, England, no. 1614). For the first 4 days, the medium was also supplemented with 2 μM XAV939 (Tocris Bioscience, no. 3748). On day 19, NPCs were dissociated with StemPro Accutase (Thermo Fisher Scientific, no. A1110501) and replated onto Matrigel for expansion. NPCs were passaged every 6 days and maintained in NPC medium (DMEM/F12, N2 supplement, B27 supplement, and 20 ng/mL bFGF [Corning, Corning, NY, no. 354060]) with medium changes every other day. For direct delivery experiments, 12,000 cells were seeded in Matrigel in a 96-well plate and after 48 h were treated in triplicate with 100 pmol of 4xNLS-SpyCas9-2xNLS RNPs with the EMX1 guide RNA (spacer: 5′ GAGTCCGAGCAGAAGAAGAA) or non-targeting guide RNA (spacer: 5′ AACGACTAGTTAGGCGTGT A). In the Lipofectamine CRISPRmax group (Thermo Fisher Scientific, no. CMAX00003), 3 μg of 0xNLS-SpyCas9-2xNLS protein (18 pmol) was mixed with sgRNA (1:1 M ratio) in 8 μL OptiMEM with 6 μL of Cas9 Plus Reagent (1 μg protein:2 μL reagent) and was mixed with a second tube containing 3.6 μL CRISPRmax reagent in 8 μL OptiMEM, incubated for at least 5 min and was immediately distributed to cells in triplicate (1 μg RNP per well) according to the manufacturer's recommendations.

Cas9 RNP assembly and delivery to cells
For cell culture experiments, RNPs were prepared immediately before use at a 1.2:1 M ratio of sgRNA (Synthego, Redwood City, CA) to protein (QB3 Macrolab or Aldevron). The solution was incubated

for 5–10 min at room temperature. For nucleofection, RNPs were formed at 10 µM in 10 µL of pre-supplemented buffer (Lonza P3 Primary Cell 96-well Kit, no. V4SP-3096). A 15-µL suspension of 250,000 mouse NPCs was mixed with 10 µL RNP solution and added to the nucleofection cuvette. Nucleofection was performed using the 4D Nucleofector X Unit (Lonza, no. AAF-1003X) with pulse code EH-100 and cells were recovered with 75 µL medium per well. Nucleofected cells were then transferred to 100 µL fresh medium in 96-well plates in triplicate and allowed to grow for 5 days at 37°C before analysis by flow cytometry for tdTomato expression. For direct delivery, RNPs were formed at 10 µM in 10 µL of sterile buffer 1 (25 mM sodium phosphate [pH 7.25], 100 mM NaCl, 200 mM trehalose). After NPCs were grown for 2 days in an adherent monolayer, 10 µL was added to cell monolayer ("direct delivery") for a final concentration of 1 µM (100 pmol RNP/100 µL medium). Medium was changed 48 h post-treatment and cells were collected 5 days post-treatment for analysis by flow cytometry for tdTomato expression or 4 days post-treatment for DNA sequencing.

For *in vivo* experiments, RNPs were prepared similarly at 10 µM concentration in buffer 1 and incubated at 37°C for 10 min. RNPs were sterile filtered by centrifuging through 0.22-µm Spin-X cellulose acetate membranes (Corning CoStar, no. 32119210) at 15,000 × *g* for 1 min at 4°C. RNPs were then concentrated using 100 kDa Ultra-0.5 mL Centrifugal Filter Unit (Amicon, Burlington, MA) at 14,000 × *g* at 4°C until the final desired concentration was reached (25–100 µM, minimum 50 µL volume) and collected by centrifuging at 1,000 × *g* for 2 min. RNPs were then divided into single-use 20 µL aliquots, flash-frozen in liquid nitrogen, and stored at −80°C until the experiment. Prior to intracranial injection, RNPs were thawed, pipetted to mix, loaded into a 25 µL syringe (Hamilton, Reno, NV, no. 7654-01) and injected with custom 29-gauge CED cannulas.

AAV9 transduction

A single 50-µL aliquot of AAV9-CMV-SauCas9-U6-sgRNA or AAV9-CMV-GFP (Virovek) was thawed from −80°C and stored at 4°C. AAV9 was diluted in 1× PBS without calcium or magnesium to the desired concentration. For *in vivo* experiments, AAV was diluted on the day of surgeries to 3e-8 to 3e-9 vg/µL and stored on ice until loaded into the syringe. Five microliters were injected in each hemisphere to a final dose of 1.5e-9 to 1.5e-10 vg per hemisphere using CED conditions (0.5 µL/min). For cell culture experiments, serial dilutions were performed from 1.6e-9 to 2e-8 vg/µL (lowest MOI = 200,000) and 10 µL of each AAV dilution was added simultaneously with NPCs in PLF-coated 96-well plates in triplicate. Treated cells were maintained for 3–9 days before flow cytometry for GFP expression (transduction) and tdTomato expression (genome editing).

Empty capsid quantification by cryoelectron microscopy

AAV samples were frozen using FEI Vitrobot Mark IV cooled down to 8°C at 100% humidity. In brief, 4 µL of AAV9 capsids containing GFP or Cas9 cargo was deposited on 2/2 400 mesh C-flat grids (Electron Microscopy Sciences, Hatfield, PA, no. CF224C-50), which were

previously glow discharged at 15 mA for 15 s on PELCO easyGLOW instrument. Grids were blotted for 3 s with blot force 8 and wait time 2.5 s. Micrographs were collected manually on Talos Arctica operated at 200 kV and magnification 36,000× (pixel size 1.14 Å/pix) using a super-resolution camera setting (0.57 Å/pix) on K3 Direct Electron Detector. Micrographs were collected using SerialEM v.3.8.7 software. Capsids were counted manually by three blinded reviewers for each image and the three counts were averaged and reported as percentage empty capsids between the two groups.

RNP size and aggregation measurement by dynamic light scattering

RNPs were prepared at 25 µM, according to the methods described above for *in vivo* experiments. Approximately 40 µL of RNP was added to a disposable cuvette (ZEN0040) and inserted into the Zetasizer Nano (ZSP, Malvern, UK) then 173° scattering angle was measured at 25°C for 5 min or 37°C after incubation for 30 min. Size distribution by mass histograms are shown with estimated peak size in nanometers (nm). Each sample was analyzed three times, resulting in a histogram generated from 10 individual measurements.

Analysis of editing *in vitro*

tdTomato positivity was assessed by flow cytometry using IGI facilities on the Attune NxT (Thermo Fisher Scientific, AFC2). In brief, mouse NPCs were washed once with 1× PBS, harvested with 0.25% trypsin, neutralized with DMEM containing 10% FBS, and resuspended in 150 µL of 1× PBS per well of a round-bottom 96-well plate for analysis. The percentage of tdTomato$^+$ cells from each well was recorded. For analysis of gDNA, medium was removed, cells were rinsed once with 1× PBS, then incubated with 100 µL QuickExtract solution (Lucigen Corporation Supplier Diversity Partner QuickExtract DNA Extraction Solution 1.0, Thermo Fisher Scientific, no. QE09050) at 37°C for 5 min. The cell lysate was then moved to a thermal cycler and incubated at 65°C for 20 min and 95°C for 20 min. gDNA was used in PCR reactions to generate amplicons of approximately 150–300 bp for Illumina sequencing. A list of primers used for NGS is provided in Table S1. Sequencing was performed with Illumina MiSeq in the IGI Center for Translational Genomics and reads were analyzed in CRISPResso2 (http://crispresso.pinellolab.org/submission).[61]

Stereotaxic infusion of Cas9 RNPs and AAVs

Ai9 mice (Jackson Laboratory, Bar Harbor, ME, no. 007909) were group housed at the University of California, Berkeley, with a 12-h light-dark cycle and allowed to feed and drink *ad libitum*. Housing, maintenance, and experimentation of the mice were carried out with strict adherence to ethical regulations set forth by the Animal Care and Use Committee (ACUC) at the University of California, Berkeley. Cas9-RNP and AAVs were prepared on-site at the University of California, Berkeley, for injection into male and female tdTomato Ai9 mice aged between 2 and 5 months. All tools were autoclaved and injected materials were sterile. Mice were anesthetized with 2% isoflurane, given pre-emptive analgesics, and arranged on an Angle Two Stereotactic Frame (Leica, Nussloch, Germany). The

incision area was swabbed with three alternating wipes of 70% ethanol and betadine scrub with sterile applicators before performing minimally damaging craniotomies. The stereotaxic surgery coordinates used for targeting the striatum, relative to bregma, were +0.74 mm anteroposterior, ±1.90 mm mediolateral, −3.37 mm dorsoventral. Bilateral CED infusion of Cas9 RNPs (10–100 μM) or Cas9 AAVs (3e-8 to 3e-9 vg/μL) was performed with a syringe pump to deliver 5 μL at 0.5 μL per minute (Model 310 Plus, KD Scientific, Holliston, MA) with a step or non-step cannula. For i.c.v. infusion of Cas9 RNPs, cannulas were placed at −0.7 mm anteroposterior, ±1.2 mm mediolateral, and −2.5 mm dorsoventral according to the Paxinos atlas of the adult mouse. Post-infusion, the syringes were left in position for 2 min before slow removal from the injection site, which was then cleaned, sutured, and surgically glued. Throughout the procedure, mice were kept at 37°C for warmth and Puralube Vet Ointment (Dechra, Northwich, England, NDC no. 17033-211-38) was applied to the outside of the eyes. For i.c.v. injection of P0 neonatal mice, anesthesia was induced by hypothermia, then 4 μL of 100 μM Cas9-RNP was injected with a handheld 33-gauge needle unilaterally with 10% Fast Green dye to visualize distribution from one ventricle throughout the CNS. The needle was inserted 2 mm deep at a location approximately 0.25 mm lateral to the sagittal suture and 0.50–0.75 mm rostral to the neonatal coronal suture. RNP was slowly injected, then the needle was held in place for 15 s, and mice were monitored until recovery. For i.t. injection, anesthetized mice received a 5-, 25-, or 50-μL bolus injection of Cas9 RNP at 300 μM. The 29-gauge needle was inserted at the L6-S1 vertebral junction and angled slightly rostrally for the injection. Mice were allowed to fully recover before being transferred back to their housing. Recovery weight following all procedures was monitored daily for 1 week and mice were housed without further disruption for various time periods until tissue collection.

Tissue collection and immunostaining

At the defined study endpoints (3, 21, and 90 days post-injection), mice were placed under anesthesia and tissues were perfused with 10 mL of cold PBS and 5 mL of 4% paraformaldehyde (PFA) (Electron Microscopy Sciences, no. 15710). Brains were post-fixed overnight in 4% PFA at 4°C, rinsed 3× with PBS, then cryoprotected in 10% sucrose in PBS solution for approximately 3 days. Brains were embedded in optimal cutting temperature medium (Thermo Fisher Scientific, no. 23-730-571) and stored at −80°C. Brains were cut at 20–35-μm-thick sections using a cryostat (Leica CM3050S) and transferred to positively charged microscope slides. For immunohistochemical analysis, tissues were blocked with solution (0.3% Triton X-100, 1% bovine serum albumin [Sigma-Aldrich, no. A9418], 5% normal goat serum [Sigma-Aldrich, no. G9023]) before 4°C incubation overnight with primary antibody in blocking solution. The next day, tissues were washed three times with PBS and incubated with secondary antibodies for 1 h at room temperature. After three PBS washes, samples were incubated with DAPI solution (0.5 μg/mL, Roche LifeScience, Penzberg, Germany) as a DNA fluorescence probe for 10 min, washed three times with PBS, submerged once in deionized water, and mounted with glass coverslips in Fluoromount-G

slide mounting medium (SouthernBiotech, Birmingham, AL). Primary antibodies included rabbit polyclonal anti-S100β (1:500, Abcam, Cambridge, England, no. ab41548), rabbit polyclonal anti-Olig-2 (1:250, Millipore Sigma, Burlington, MA, no. AB9610), rabbit polyclonal anti-doublecortin (1:800, Cell Signaling Technology, Danvers, MA, no. 4604), rabbit polyclonal anti-Ki67 (1:100, Abcam, no. ab15580), mouse monoclonal anti-NeuN (1:500, Millipore Sigma, no. MAB377), rabbit polyclonal anti-DARPP-32 (1:100, Cell Signaling Technology, no. 2302), rabbit polyclonal anti-Iba1 (1:100, Wako Chemicals, Richmond, VA, no. 019–19741), mouse monoclonal anti-glial fibrillary acidic protein (1:1,000, Millipore Sigma, no. MAB3402), rat monoclonal anti-CD45 (1:200, Thermo Fisher Scientific, no. RA3-6B2), and rabbit polyclonal anti-CD3 (1:150, Abcam, no. ab5690). Secondary antibodies included donkey anti-rat 488 (1:500, Thermo Fisher Scientific, no. A-21208), goat anti-rabbit 488 (1:500, Thermo Fisher Scientific, no. A32731), goat anti-rabbit 647 (1:500, Thermo Fisher Scientific, no. A21245), and goat anti-mouse IgG1 647 (1:500, Thermo Fisher Scientific, no. A-21240).

Fluorescent imaging and image quantification

Whole-brain sections were imaged and stitched using the automated AxioScanZ1 (Zeiss, Oberkochen, Germany) with a 20× objective in the DAPI and tdTomato channels. Images generated from slide scanning were viewed in ZenLite software (v.3.6 blue edition) as CZI files. Images were then exported to FIJI (v.1.53q), Imaris (v.9.9.1), or QuPath (v.0.3.2) for quantification by authors blinded to the sample identity. The area of reflux from CED needles was calculated directly in ZenLite using the shape and area analysis tools. Immunostained cells and tissues were imaged on the Evos Revolve widefield microscope using a 20× objective or Stellaris 5 confocal microscope (Leica) with a 10× or 25× water immersion objective to capture data in DAPI, FITC, tdTomato, and CY5 channels. Approximately four images were taken at 20–25× per hemisphere across multiple sections for image quantification of CD45, Iba1, and CD3 (8–12 images quantified and averaged per injection). Approximately four to six z stack images were captured and stitched per hemisphere for qualitative images of Iba1 and for quantification of NeuN, DARPP-32, ALDH1L1, and OLIG2 with tdTomato at 1,024 × 1,024 pixel resolution with a scanning speed of 100–200.

Measurements of striatal editing by volume were conducted using QuPath software (v.0.3.2) from images obtained from the Zeiss AxioscanZ1. In brief, ROIs were drawn to outline the border of each striatum and the inner area of tdTomato editing using the polygon tool to create annotations. All coronal plane areas were automatically calculated. Dorsoventral coordinates (relative to bregma) were then estimated in millimeters by consulting the Mouse Brain Atlas (C57BL/6J Coronal). Approximate tissue volume was calculated by averaging outlined areas between consecutive sections to represent the mean area across a dorsoventral segment and multiplying by the difference in dorsoventral coordinates. Edited striatal volumes were then divided by total striatal volumes to obtain percent editing. Additional tdTomato$^+$ cell count measurements were conducted in Imaris software v.10.0 (Oxford Instruments, Abingdon, UK). In brief,

ROIs were drawn over each hemisphere (including cells in all brain sub-structures) using the "Segment only a Region of Interest" tool, and positive cells detected using the automated "Spots" tool to provide cell counts. Thresholds were adjusted manually. Counts of tdTomato cells on each image were then related back to approximate coordinates relative to bregma using the Mouse Brain Atlas (C57BL/6J Coronal) to quantify the distribution of edited cells.

Cell-type-specific measurements were conducted using QuPath software (v.0.3.2) on images obtained from Stellaris 5 z stack maximal projections. ROIs were again drawn around areas of observed tdTomato editing, using the polygon tool to create a single annotation per image. Cell count calculations were performed using the "Cell Detection" and "Positive Cell Detection" tools, adjusting "Cell Mean" thresholds accordingly for each channel and image. Percent area and intensity measurements were performed in FIJI/ImageJ software (v.2.1.0/1.53c). Images were converted to 32-bit, and thresholds were adjusted to detect the corresponding stained area. Measurements were set to include area, minimum, maximum, and mean gray value, and area fraction, as well as to limit to threshold. All image quantification was performed on two to five serial sections with three to ten independent injections per group for each analysis. Cell counts, area, intensity, and volume measurements were in general averaged from multiple sections and then grouped with other biological and technical replicates, to report the treatment group average with standard deviation displayed by bar graph or box and whisker plot.

Serum collection and ELISA

Blood was collected from mice at the time of euthanasia, allowed to clot at room temperature for 15–30 min, then centrifuged for 5 min at $2,000 \times g$. Serum was collected and placed immediately on dry ice and then stored at $-80°C$. Enzyme-linked immunosorbent assays were performed using the SeraCare Protein Detector HRP Microwell Anti-Mouse ELISA Kit, no. 5110-0011 (54-62-18) according to the manufacturer's recommendations. First, 96-well plates were coated with antigens of interest (0.5 μg protein per well for SauCas9 and SpyCas9 (4xNLS protein variants) and approximately 1e-9 empty AAV capsids per well) overnight at 4°C. Wells were washed three times and blocked at room temperature for 1 h. Serum samples were then incubated in wells at varying concentrations (1:50 to 1:10,000 dilution) in $1\times$ blocking buffer for 4 h at room temperature, along with monoclonal antibody controls to generate standard curves. Standards included CRISPR-Cas9 Monoclonal Antibody 7A9 (Epigentek, Farmingdale, NY, no. A-9000-050), GenCRISPR SaCas9 Antibody 26H10 (GenScript, Piscataway, NJ, no. A01952), and Anti-Adeno-associated Virus 9 Antibody clone HL2374 (Millipore Sigma, no. MABF2326-25UG). Following three additional washes, the HRP secondary antibody was added at 1:500 in $1\times$ blocking buffer and incubated for 1 h. Wells were then washed three more times, and peroxidase substrate solutions were added. Absorbance was recorded at a wavelength of 405 nm with Cytation5 plate reader with Gen 5 3.04 software (BioTek). Serum antibody concentrations were calculated using four-parameter logistic curve data analysis (4PL, MyAssays. com) and normalized to sham controls.

Splenocyte collection and ELISpot

Spleens were collected at the time of euthanasia and stored in medium composed of RPMI 1640 (Thermo Fisher Scientific, no. 11875-119) with 10% FBS (VWR, no. 89510-186, Radnor, PA) and 1% Pen/Strep (Thermo Fisher Scientific, no. 15140-122). In brief, spleens were physically dissociated with a 100-μm cell strainer in 10 mL of medium then single cells were passed through a 70-μm strainer and centrifuged at $200 \times g$ for 5 min. Cells were resuspended in 5 mL of $1\times$ RBC Lysis Buffer (Miltenyi, no. 130-094-183) for approximately 3 min, then centrifuged again and resuspended in medium for counting. The mouse IFN-γ ELISpot kit (R&D Systems, Minneapolis, MN, no. EL485) was used according to the manufacturer's instructions to assess activation of splenocytes, containing T cells, in response to treatment with Cas9 proteins. In brief, the plate was pre-incubated with 200 μL of medium for at least 20 min, before adding cells at 300,000 per well in 100 μL medium. Treatments at $2\times$ dose were prepared in medium and 100 μL was added to wells in triplicate (final 5 μg/mL concentration). Plates were incubated for 48 h without disturbing. Concanavalin A (Sigma-Aldrich, no. C5275) was used as a positive control for cell-mediated IFN-γ production (final 4 μg/mL concentration). After 48 h, cells were removed and the secreted analyte was detected with immunostaining using the kit-provided biotinylated monoclonal antibody specific for mouse IFN-γ, streptavidin-conjugated alkaline phosphatase, and stabilized detection mixture of 5-bromo-4-chloro-3′-indolylphosphate-p-toluidine salt and nitro blue tetrazolium chloride. After staining, plates were dried overnight and spot forming units were imaged and counted on the ImmunoSpot S6 Macro Analyzer (Cellular Technology Limited, Shaker Heights, OH).

Pre-treatment of mice with Cas9 and adjuvant

AddaVax (Invivogen, vac-adx-10), a squalene-based oil-in-water nano-emulsion, was mixed with an equal volume containing 25 μg of 4x-SpyCas9-2x protein diluted in sterile buffer at room temperature for a final injection volume of 50 μL. Mice received two 25 μL subcutaneous injections of the AddaVax:Cas9 mixture (immunized) or AddaVax:Buffer alone (sham) with a 30-gauge insulin syringe into each flank. After 4 weeks, stereotaxic surgery with bilateral injections of 5 μL of 25 μM Cas9-RNPs was performed in a subset of the mice. Mice showed no signs of pain or distress following treatment with AddaVax and no acute events were noted after surgery. Mice that received AddaVax, with or without surgery, were euthanized 6 weeks post-subcutaneous injections. Brains, serum, and spleens were collected for analysis of adaptive immune responses against repeated exposure to Cas9.

DNA/RNA extraction from brain tissue slices and qRT-PCR, ddPCR, and long-read sequencing

Brains were collected at 3, 28, or 120 days (4 months) for DNA and RNA analysis. In brief, mice were placed under anesthesia and perfused with cold PBS. Brains were harvested and cut into 2-mm sections using a matrix around the injection site (Zivic Instruments, Pittsburgh, PA). The slices were transferred onto chilled glass slides and further trimmed to approximate 30 mg tissue weight

(1–1.25 mm wide × 2 mm long). Tissues were flash frozen in liquid nitrogen then stored at −80°C until processing. DNA and RNA were collected from tissues using the AllPrep DNA/RNA Mini Kit (-QIAGEN, Venlo, the Netherlands, no. 80204) according to the manufacturer's instructions. In brief, brains were homogenized in 1.5-mL tubes with a disposable pestle directly in RLT lysis buffer supplemented with 2-mercaptoethanol, then passed through Qiashredder columns before adding directly to the DNA and RNA binding columns. DNA was eluted in 100 μL of EB and RNA was eluted in 40 μL RNAse-free water. Concentrations of nucleic acids were measured using a NanoDrop spectrophotometer and samples were stored at −20°C.

Gene expression was quantified across multiple samples using a Custom RT^2 PCR Array (QIAGEN, no. 330171, CLAM45824) and analyzed using the RT^2 Profiler PCR Data Analysis Tool on GeneGlobe (QIAGEN). For reverse transcription, the RT^2 First Strand Kit (QIAGEN, no. 330404) was used according to the manufacturer's instructions. cDNA was diluted in water and added to the RT^2 SYBR Green qPCR Mastermix (QIAGEN, no. 330502) then distributed across the 24-wells containing verified assay primers and controls (PCR array reproducibility control, reverse transcription efficiency control, gDNA contamination control, two housekeeping genes, and 19 experimental genes). Quantitative real-time PCR was performed on the CFX96 Touch Real-Time PCR System (Bio-Rad). cDNA was also used in a ddPCR reaction to measure SauCas9 expression at the 4-month time point. qPCR assay IDs are included in Tables S1 and S2.

Off-target sites were predicted using Cas-OFFinder (http://www.rgenome.net/cas-offinder/),[62] described further in Tables S3 and S4. Primers were designed using NCBI Primer Blast with an amplicon size of 250–300 bp, listed in Table S1. Sequencing was performed with Illumina MiSeq in the IGI Center for Translational Genomics and reads were analyzed in CRISPResso2 (http://crispresso.pinellolab.org).[61]

For ddPCR, custom NHEJ ddPCR assays were generated using the online Bio-Rad design tool (Table S2). Assays for SauCas9 and SpyCas9 contain both the primers and probes (HEX-probe spanning the cut-site and a distal reference FAM-probe). To prepare the reactions, 110 ng of gDNA was combined with the 20× assay, 2× ddPCR Supermix for Probes (No dUTP), 1 μL of SmaI restriction enzyme (2 units per reaction), and water up to 22 μL. Then 20 μL of each reaction mix was added to DG8TM Cartridges (Bio-Rad, Hercules, CA, no. 1864008) followed by 70 μL of Droplet Generation Oil for Probes (Bio-Rad, no. 1863005) and droplets were formed in the QX200 Droplet Generator. Droplets were then transferred to a 96-well plate and thermal cycled according to the manufacturer's recommendation with a 3-min annealing/extension step. After thermal cycling, the sealed plate was placed in the QX200 Droplet Reader and data were acquired and analyzed in the QuantaSoft Analysis Pro Software using the "Drop-Off" analysis, manually setting the thresholds for cluster calling (FAM+ only,

FAM+ HEX+ cluster, FAM–HEX– cluster), and exporting fractional abundance calculations.

Long-read sequencing of the tdTomato locus was performed on DNA isolated from the treated mouse brains. In brief, PCR amplicons were generated on samples from the 4-month treatment groups using primers with unique barcodes for sample de-multiplexing. The KAPA HiFi Hotstart PCR Kit (Roche, KK2502) was used to amplify the 1,100-bp product and reactions were cleaned with AMPure XP magnetic beads (Beckman Coulter, Brea, CA) before analysis by Qubit and Bioanalyzer with the DNA 7500 Kit (Agilent, Santa Clara, CA, no. 5067-1506). Samples were combined with 1 μg of pooled amplicons and submitted (>20 ng/μL) for sequencing with one PacBio Sequel 8M SMRT Cell at the QB3 Vincent Coates Genomic Sequencing Lab, yielding approximately 110,000 reads per sample. Data were analyzed using a custom pipeline to identify viral fragment trapping during DNA repair. In brief, PacBio circular consensus reads were trimmed with Cutadapt (v,4.1),[63] then aligned to the AAV vector using NGMLR (v,0.2.7)[64] to generate BAM files. Soft-clipped regions of aligned reads were extracted using PySam (v,0.18.0, https://github.com/pysam-developers/pysam) to parse CIGAR strings, then realigned to the tdTomato locus with NGMLR to verify integration within 200 bp of the cut site. Confirmed integrations were visualized along the AAV genome using pyGenomeTracks (v.3.3) and coverage statistics were summarized using PySam.[65,66]

Statistical analyses
The data presented in bar graphs and box and whisker plots are averages across multiple technical and biological replicates and error bars represent the standard deviation. Sample sizes are indicated in the text and figure legends (generally bilateral injections were treated independently, i.e., two technical replicates per one biological replicate). When comparing two groups with normal distribution, an unpaired Student's t test was performed in Prism 9 (GraphPad Software v.9.4.1). When comparing multiple groups, a one-way ANOVA with Tukey's multiple comparison test was performed in Prism 9 (GraphPad Software v.9.4.1). The qRT-PCR experiments used Student's t test of the experimental group compared with the sham control (QIAGEN GeneGlobe RT^2 Profiler PCR Data Analysis). $p \leq 0.05$ was considered significant.

DATA AVAILABILITY
Long-read sequencing (BAM files from PacBio circular consensus sequence) are available in Sequence Read Archive: PRJNA986952. All additional data are available upon request.

SUPPLEMENTAL INFORMATION
Supplemental information can be found online at https://doi.org/10.1016/j.ymthe.2023.06.019.

AUTHOR CONTRIBUTIONS

E.C.S. performed the experiments, analysis, and manuscript preparation and oversaw contributions from researchers (R.A., E.A., S.E.K., A.S., N.L., and Y.K.) who assisted with tissue processing, cloning, ELISAs, immunohistochemistry, and image analysis. E.C.S., J.K.S., and M.H.K. designed *in vivo* experiments, performed stereotaxic surgeries, confocal microscopy, and quantitative PCR. M.T. performed long-read NGS sequencing analysis. E.C.S. performed isolation and culture of mouse primary cells, flow cytometry, and ELISpot assays. K.M.S. performed electron microscopy. V.S.-R. and L.T.V. performed human stem cell culture and differentiation. C.J., A.W., T.M., A.K., and T.F. performed custom low endotoxin protein expression and purification. D.F.S. and J.A.D. approved the experiments, provided intellectual contributions, and co-wrote the manuscript.

DECLARATION OF INTERESTS

REFERENCES

1. Heidenreich, M., and Zhang, F. (2016). Applications of CRISPR–Cas systems in neuroscience. Nat. Rev. Neurosci. *17*, 36–44. https://doi.org/10.1038/nrn.2015.2.

2. Saha, K., Sontheimer, E.J., Brooks, P.J., Dwinell, M.R., Gersbach, C.A., Liu, D.R., Murray, S.A., Tsai, S.Q., Wilson, R.C., Anderson, D.G., et al. (2021). The NIH Somatic Cell Genome Editing program. Nature *592*, 195–204. https://doi.org/10.1038/s41586-021-03191-1.

3. Jinek, M., Chylinski, K., Fonfara, I., Hauer, M., Doudna, J.A., and Charpentier, E. (2012). A Programmable Dual-RNA–Guided DNA Endonuclease in Adaptive Bacterial Immunity. Science *337*, 816–821. https://doi.org/10.1126/science.1225829.

4. Jinek, M., East, A., Cheng, A., Lin, S., Ma, E., and Doudna, J. (2013). RNA-programmed genome editing in human cells. eLife *2*, e00471. https://doi.org/10.7554/eLife.00471.

5. Doudna, J.A. (2020). The promise and challenge of therapeutic genome editing. Nature *578*, 229–236. https://doi.org/10.1038/s41586-020-1978-5.

6. Hadaczek, P., Forsayeth, J., Mirek, H., Munson, K., Bringas, J., Pivirotto, P., McBride, J.L., Davidson, B.L., and Bankiewicz, K.S. (2009). Transduction of Nonhuman Primate Brain with Adeno-Associated Virus Serotype 1: Vector Trafficking and Immune Response. Hum. Gene Ther. *20*, 225–237. https://doi.org/10.1089/hum.2008.151.

7. Ciesielska, A., Hadaczek, P., Mittermeyer, G., Zhou, S., Wright, J.F., Bankiewicz, K.S., and Forsayeth, J. (2013). Cerebral Infusion of AAV9 Vector-encoding Non-self Proteins Can Elicit Cell-mediated Immune Responses. Mol. Ther. *21*, 158–166. https://doi.org/10.1038/mt.2012.167.

8. Samaranch, L., Sebastian, W.S., Kells, A.P., Salegio, E.A., Heller, G., Bringas, J.R., Pivirotto, P., DeArmond, S., Forsayeth, J., and Bankiewicz, K.S. (2014). AAV9-mediated Expression of a Non-self Protein in Nonhuman Primate Central Nervous System Triggers Widespread Neuroinflammation Driven by Antigen-presenting Cell Transduction. Mol. Ther. *22*, 329–337. https://doi.org/10.1038/mt.2013.266.

9. Agustín-Pavón, C., Mielcarek, M., Garriga-Canut, M., and Isalan, M. (2016). Deimmunization for gene therapy: host matching of synthetic zinc finger constructs enables long-term mutant Huntingtin repression in mice. Mol. Neurodegener. *11*, 64. https://doi.org/10.1186/s13024-016-0128-x.

10. Chew, W.L., Tabebordbar, M., Cheng, J.K.W., Mali, P., Wu, E.Y., Ng, A.H.M., Zhu, K., Wagers, A.J., and Church, G.M. (2016). A multifunctional AAV–CRISPR–Cas9 and its host response. Nat. Methods *13*, 868–874. https://doi.org/10.1038/nmeth.3993.

11. Moreno, A.M., Palmer, N., Alemán, F., Chen, G., Pla, A., Jiang, N., Leong Chew, W., Law, M., and Mali, P. (2019). immune-orthogonal orthologues of AAV capsids and of Cas9 circumvent the immune response to the administration of gene therapy. Nat. Biomed. Eng. *3*, 806–816. https://doi.org/10.1038/s41551-019-0431-2.

12. Li, A., Tanner, M.R., Lee, C.M., Hurley, A.E., De Giorgi, M., Jarrett, K.E., Davis, T.H., Doerfler, A.M., Bao, G., Beeton, C., and Lagor, W.R. (2020). AAV-CRISPR Gene Editing Is Negated by Pre-existing Immunity to Cas9. Mol. Ther. *28*, 1432–1441. https://doi.org/10.1016/j.ymthe.2020.04.017.

13. Simhadri, V.L., McGill, J., McMahon, S., Wang, J., Jiang, H., and Sauna, Z.E. (2018). Prevalence of Pre-existing Antibodies to CRISPR-Associated Nuclease Cas9 in the USA Population. Mol. Ther. Methods Clin. Dev. *10*, 105–112. https://doi.org/10.1016/j.omtm.2018.06.006.

14. Charlesworth, C.T., Deshpande, P.S., Dever, D.P., Camarena, J., Lemgart, V.T., Cromer, M.K., Vakulskas, C.A., Collingwood, M.A., Zhang, L., Bode, N.M., et al. (2019). Identification of preexisting adaptive immunity to Cas9 proteins in humans. Nat. Med. *25*, 249–254. https://doi.org/10.1038/s41591-018-0326-x.

15. Wagner, D.L., Amini, L., Wendering, D.J., Burkhardt, L.-M., Akyüz, L., Reinke, P., Volk, H.-D., and Schmueck-Henneresse, M. (2019). High prevalence of Streptococcus pyogenes Cas9-reactive T cells within the adult human population. Nat. Med. *25*, 242–248. https://doi.org/10.1038/s41591-018-0204-6.

16. Ferdosi, S.R., Ewaisha, R., Moghadam, F., Krishna, S., Park, J.G., Ebrahimkhani, M.R., Kiani, S., and Anderson, K.S. (2019). Multifunctional CRISPR-Cas9 with engineered immunosilenced human T cell epitopes. Nat. Commun. *10*, 1842. https://doi.org/10.1038/s41467-019-09693-x.

17. Tang, X.-Z.E., Tan, S.X., Hoon, S., and Yeo, G.W. (2022). Pre-existing adaptive immunity to the RNA-editing enzyme Cas13d in humans. Nat. Med. 28, 1372–1376. https://doi.org/10.1038/s41591-022-01848-6.

18. Mingozzi, F., and High, K.A. (2013). Immune responses to AAV vectors: overcoming barriers to successful gene therapy. Blood 122, 23–36. https://doi.org/10.1182/blood-2013-01-306647.

19. Staahl, B.T., Benekareddy, M., Coulon-Bainier, C., Banfal, A.A., Floor, S.N., Sabo, J.K., Urnes, C., Munares, G.A., Ghosh, A., and Doudna, J.A. (2017). Efficient genome editing in the mouse brain by local delivery of engineered Cas9 ribonucleoprotein complexes. Nat. Biotechnol. 35, 431–434. https://doi.org/10.1038/nbt.3806.

20. Liu, J., Gaj, T., Wallen, M.C., and Barbas, C.F. (2015). Improved Cell-Penetrating Zinc-Finger Nuclease Proteins for Precision Genome Engineering. Mol. Ther. Nucleic Acids 4, e232. https://doi.org/10.1038/mtna.2015.6.

21. Madisen, L., Zwingman, T.A., Sunkin, S.M., Oh, S.W., Zariwala, H.A., Gu, H., Ng, L.L., Palmiter, R.D., Hawrylycz, M.J., Jones, A.R., et al. (2010). A robust and high-throughput Cre reporting and characterization system for the whole mouse brain. Nat. Neurosci. 13, 133–140. https://doi.org/10.1038/nn.2467.

22. Ran, F.A., Cong, L., Yan, W.X., Scott, D.A., Gootenberg, J.S., Kriz, A.J., Zetsche, B., Shalem, O., Wu, X., Makarova, K.S., et al. (2015). In vivo genome editing using Staphylococcus aureus Cas9. Nature 520, 186–191. https://doi.org/10.1038/nature14299.

23. Maeder, M.L., Stefanidakis, M., Wilson, C.J., Baral, R., Barrera, L.A., Bounoutas, G.S., Bumcrot, D., Chao, H., Ciulla, D.M., DaSilva, J.A., et al. (2019). Development of a gene-editing approach to restore vision loss in Leber congenital amaurosis type 10. Nat. Med. 25, 229–233. https://doi.org/10.1038/s41591-018-0327-9.

24. Yin, C., Zhang, T., Qu, X., Zhang, Y., Putatunda, R., Xiao, X., Li, F., Xiao, W., Zhao, H., Dai, S., et al. (2017). In Vivo Excision of HIV-1 Provirus by saCas9 and Multiplex Single-Guide RNAs in Animal Models. Mol. Ther. 25, 1168–1186. https://doi.org/10.1016/j.ymthe.2017.03.012.

25. Gao, G., Vandenberghe, L.H., Alvira, M.R., Lu, Y., Calcedo, R., Zhou, X., and Wilson, J.M. (2004). Clades of Adeno-Associated Viruses Are Widely Disseminated in Human Tissues. J. Virol. 78, 6381–6388. https://doi.org/10.1128/JVI.78.12.6381-6388.2004.

26. Smith, R.H., Levy, J.R., and Kotin, R.M. (2009). A Simplified Baculovirus-AAV Expression Vector System Coupled With One-step Affinity Purification Yields High-titer rAAV Stocks From Insect Cells. Mol. Ther. 17, 1888–1896. https://doi.org/10.1038/mt.2009.128.

27. Chen, C., Akerstrom, V., Baus, J., Lan, M.S., and Breslin, M.B. (2013). Comparative analysis of the transduction efficiency of five adeno associated virus serotypes and VSV-G pseudotype lentiviral vector in lung cancer cells. Virol. J. 10, 86. https://doi.org/10.1186/1743-422X-10-86.

28. Gaj, T., Staahl, B.T., Rodrigues, G.M.C., Limsirichai, P., Ekman, F.K., Doudna, J.A., and Schaffer, D.V. (2017). Targeted gene knock-in by homology-directed genome editing using Cas9 ribonucleoprotein and AAV donor delivery. Nucleic Acids Res. 45, e98. https://doi.org/10.1093/nar/gkx154.

29. Park, I.-H., Zhao, R., West, J.A., Yabuuchi, A., Huo, H., Ince, T.A., Lerou, P.H., Lensch, M.W., and Daley, G.Q. (2008). Reprogramming of human somatic cells to pluripotency with defined factors. Nature 451, 141–146. https://doi.org/10.1038/nature06534.

30. Qi, Y., Zhang, X.-J., Renier, N., Wu, Z., Atkin, T., Sun, Z., Ozair, M.Z., Tchieu, J., Zimmer, B., Fattahi, F., et al. (2017). Combined small-molecule inhibition accelerates the derivation of functional cortical neurons from human pluripotent stem cells. Nat. Biotechnol. 35, 154–163. https://doi.org/10.1038/nbt.3777.

31. Chambers, S.M., Fasano, C.A., Papapetrou, E.P., Tomishima, M., Sadelain, M., and Studer, L. (2009). Highly efficient neural conversion of human ES and iPS cells by dual inhibition of SMAD signaling. Nat. Biotechnol. 27, 275–280. https://doi.org/10.1038/nbt.1529.

32. Fu, Y., Foden, J.A., Khayter, C., Maeder, M.L., Reyon, D., Joung, J.K., and Sander, J.D. (2013). High-frequency off-target mutagenesis induced by CRISPR-Cas nucleases in human cells. Nat. Biotechnol. 31, 822–826. https://doi.org/10.1038/nbt.2623.

33. Bobo, R.H., Laske, D.W., Akbasak, A., Morrison, P.F., Dedrick, R.L., and Oldfield, E.H. (1994). Convection-enhanced delivery of macromolecules in the brain. Proc. Natl. Acad. Sci. USA. 91, 2076–2080. https://doi.org/10.1073/pnas.91.6.2076.

34. Hadaczek, P., Kohutnicka, M., Krauze, M.T., Bringas, J., Pivirotto, P., Cunningham, J., and Bankiewicz, K. (2006). Convection-Enhanced Delivery of Adeno-Associated Virus Type 2 (AAV2) into the Striatum and Transport of AAV2 Within Monkey Brain. Hum. Gene Ther. 17, 291–302. https://doi.org/10.1089/hum.2006.17.291.

35. Krauze, M.T., Saito, R., Noble, C., Tamas, M., Bringas, J., Park, J.W., Berger, M.S., and Bankiewicz, K. (2005). Reflux-free cannula for convection-enhanced high-speed delivery of therapeutic agents: Technical note. J. Neurosurg. 103, 923–929. https://doi.org/10.3171/jns.2005.103.5.0923.

36. Aschauer, D.F., Kreuz, S., and Rumpel, S. (2013). Analysis of Transduction Efficiency, Tropism and Axonal Transport of AAV Serotypes 1, 2, 5, 6, 8 and 9 in the Mouse Brain. PLoS ONE 8, e76310. https://doi.org/10.1371/journal.pone.0076310.

37. Hanlon, K.S., Kleinstiver, B.P., Garcia, S.P., Zaborowski, M.P., Volak, A., Spirig, S.E., Muller, A., Sousa, A.A., Tsai, S.Q., Bengtsson, N.E., et al. (2019). High levels of AAV vector integration into CRISPR-induced DNA breaks. Nat. Commun. 10, 4439. https://doi.org/10.1038/s41467-019-12449-2.

38. Nelson, C.E., Wu, Y., Gemberling, M.P., Oliver, M.L., Waller, M.A., Bohning, J.D., Robinson-Hamm, J.N., Bulaklak, K., Castellanos Rivera, R.M., Collier, J.H., et al. (2019). Long-term evaluation of AAV-CRISPR genome editing for Duchenne muscular dystrophy. Nat. Med. 25, 427–432. https://doi.org/10.1038/s41591-019-0344-3.

39. Ferrari, S., Jacob, A., Cesana, D., Laugel, M., Beretta, S., Varesi, A., Unali, G., Conti, A., Canarutto, D., Albano, L., et al. (2022). Choice of template delivery mitigates the genotoxic risk and adverse impact of editing in human hematopoietic stem cells. Cell Stem Cell 29, 1428–1444.e9. https://doi.org/10.1016/j.stem.2022.09.001.

40. Simpson, B.P., Yrigollen, C.M., Izda, A., and Davidson, B.L. (2023). Targeted long-read sequencing captures CRISPR editing and AAV integration outcomes in brain. Mol. Ther. 31, 760–773. S1525001623000047. https://doi.org/10.1016/j.ymthe.2023.01.004.

41. Zink McCullough, K. Calculating Endotoxin Limits for Drug Products (American Pharmaceutical Review).

42. Lee, B., Lee, K., Panda, S., Gonzales-Rojas, R., Chong, A., Bugay, V., Park, H.M., Brenner, R., Murthy, N., and Lee, H.Y. (2018). Nanoparticle delivery of CRISPR into the brain rescues a mouse model of fragile X syndrome from exaggerated repetitive behaviours. Nat. Biomed. Eng. 2, 497–507. https://doi.org/10.1038/s41551-018-0252-8.

43. Park, H., Oh, J., Shim, G., Cho, B., Chang, Y., Kim, S., Baek, S., Kim, H., Shin, J., Choi, H., et al. (2019). In vivo neuronal gene editing via CRISPR–Cas9 amphiphilic nanocomplexes alleviates deficits in mouse models of Alzheimer's disease. Nat. Neurosci. 22, 524–528. https://doi.org/10.1038/s41593-019-0352-0.

44. Metzger, J.M., Wang, Y., Neuman, S.S., Snow, K.J., Murray, S.A., Lutz, C.M., Bondarenko, V., Felton, J., Gimse, K., Xie, R., et al. (2023). Efficient in vivo neuronal genome editing in the mouse brain using nanocapsules containing CRISPR-Cas9 ribonucleoproteins. Biomaterials 293, 121959. https://doi.org/10.1016/j.biomaterials.2022.121959.

45. Wang, Y., Wang, X., Xie, R., Burger, J.C., Tong, Y., and Gong, S. (2023). Overcoming the Blood–Brain Barrier for Gene Therapy via Systemic Administration of GSH-Responsive Silica Nanocapsules. Adv. Mater. 35, 2208018. https://doi.org/10.1002/adma.202208018.

46. Yan, S., Zheng, X., Lin, Y., Li, C., Liu, Z., Li, J., Tu, Z., Zhao, Y., Huang, C., Chen, Y., et al. (2023). Cas9-mediated replacement of expanded CAG repeats in a pig model of Huntington's disease. Nat. Biomed. Eng. 7, 629–646. https://doi.org/10.1038/s41551-023-01007-3.

47. He, M., Li, J., Han, H., Borges, C.A., Neiman, G., Røise, J.J., Hadaczek, P., Mendonsa, R., Holm, V.R., Wilson, R.C., et al. (2020). A traceless linker for aliphatic amines that rapidly and quantitatively fragments after reduction. Chem. Sci. 11, 8973–8980. https://doi.org/10.1039/D0SC00929F.

48. Saito, R., Krauze, M.T., Noble, C.O., Tamas, M., Drummond, D.C., Kirpotin, D.B., Berger, M.S., Park, J.W., and Bankiewicz, K.S. (2006). Tissue affinity of the infusate affects the distribution volume during convection-enhanced delivery into rodent brains: Implications for local drug delivery. J. Neurosci. Methods 154, 225–232. https://doi.org/10.1016/j.jneumeth.2005.12.027.

49. Wei, T., Cheng, Q., Min, Y.-L., Olson, E.N., and Siegwart, D.J. (2020). Systemic nanoparticle delivery of CRISPR-Cas9 ribonucleoproteins for effective tissue specific

genome editing. Nat. Commun. *11*, 3232. https://doi.org/10.1038/s41467-020-17029-3.

50. Oura, S., Noda, T., Morimura, N., Hitoshi, S., Nishimasu, H., Nagai, Y., Nureki, O., and Ikawa, M. (2021). Precise CAG repeat contraction in a Huntington's Disease mouse model is enabled by gene editing with SpCas9-NG. Commun. Biol. *4*, 771. https://doi.org/10.1038/s42003-021-02304-w.

51. Sweeney, M.D., Sagare, A.P., and Zlokovic, B.V. (2018). Blood–brain barrier breakdown in Alzheimer disease and other neurodegenerative disorders. Nat. Rev. Neurol. *14*, 133–150. https://doi.org/10.1038/nrneurol.2017.188.

52. Huang, L., Bommireddy, R., Munoz, L.E., Guin, R.N., Wei, C., Ruggieri, A., Menon, A.P., Li, X., Shanmugam, M., Owonikoko, T.K., et al. (2021). Expression of tdTomato and luciferase in a murine lung cancer alters the growth and immune microenvironment of the tumor. PLoS One *16*, e0254125. https://doi.org/10.1371/journal.pone.0254125.

53. Tsai, S.Q., Zheng, Z., Nguyen, N.T., Liebers, M., Topkar, V.V., Thapar, V., Wyvekens, N., Khayter, C., Iafrate, A.J., Le, L.P., et al. (2015). GUIDE-seq enables genome-wide profiling of off-target cleavage by CRISPR-Cas nucleases. Nat. Biotechnol. *33*, 187–197. https://doi.org/10.1038/nbt.3117.

54. Tsai, S.Q., Nguyen, N.T., Malagon-Lopez, J., Topkar, V.V., Aryee, M.J., and Joung, J.K. (2017). CIRCLE-seq: a highly sensitive in vitro screen for genome-wide CRISPR–Cas9 nuclease off-targets. Nat. Methods *14*, 607–614. https://doi.org/10.1038/nmeth.4278.

55. Ibraheim, R., Tai, P.W.L., Mir, A., Javeed, N., Wang, J., Rodríguez, T.C., Namkung, S., Nelson, S., Khokhar, E.S., Mintzer, E., et al. (2021). Self-inactivating, all-in-one AAV vectors for precision Cas9 genome editing via homology-directed repair in vivo. Nat. Commun. *12*, 6267. https://doi.org/10.1038/s41467-021-26518-y.

56. Li, A., Lee, C.M., Hurley, A.E., Jarrett, K.E., De Giorgi, M., Lu, W., Balderrama, K.S., Doerfler, A.M., Deshmukh, H., Ray, A., et al. (2019). A Self-Deleting AAV-CRISPR System for In Vivo Genome Editing. Mol. Ther. Methods Clin. Dev. *12*, 111–122. https://doi.org/10.1016/j.omtm.2018.11.009.

57. Merienne, N., Vachey, G., de Longprez, L., Meunier, C., Zimmer, V., Perriard, G., Canales, M., Mathias, A., Herrgott, L., Beltraminelli, T., et al. (2017). The Self-Inactivating KamiCas9 System for the Editing of CNS Disease Genes. Cell Rep. *20*, 2980–2991. https://doi.org/10.1016/j.celrep.2017.08.075.

58. Ewaisha, R., and Anderson, K.S. (2023). Immunogenicity of CRISPR therapeutics—Critical considerations for clinical translation. Front. Bioeng. Biotechnol. *11*, 1138596. https://doi.org/10.3389/fbioe.2023.1138596.

59. Mancuso, P., Chen, C., Kaminski, R., Gordon, J., Liao, S., Robinson, J.A., Smith, M.D., Liu, H., Sariyer, I.K., Sariyer, R., et al. (2020). CRISPR based editing of SIV proviral DNA in ART treated non-human primates. Nat. Commun. *11*, 6065. https://doi.org/10.1038/s41467-020-19821-7.

60. Harrington, L.B., Paez-Espino, D., Staahl, B.T., Chen, J.S., Ma, E., Kyrpides, N.C., and Doudna, J.A. (2017). A thermostable Cas9 with increased lifetime in human plasma. Nat. Commun. *8*, 1424. https://doi.org/10.1038/s41467-017-01408-4.

61. Clement, K., Rees, H., Canver, M.C., Gehrke, J.M., Farouni, R., Hsu, J.Y., Cole, M.A., Liu, D.R., Joung, J.K., Bauer, D.E., and Pinello, L. (2019). CRISPResso2 provides accurate and rapid genome editing sequence analysis. Nat. Biotechnol. *37*, 224–226. https://doi.org/10.1038/s41587-019-0032-3.

62. Bae, S., Park, J., and Kim, J.-S. (2014). Cas-OFFinder: a fast and versatile algorithm that searches for potential off-target sites of Cas9 RNA-guided endonucleases. Bioinformatics *30*, 1473–1475. https://doi.org/10.1093/bioinformatics/btu048.

63. Martin, M. (2011). Cutadapt removes adapter sequences from high-throughput sequencing reads. Embnet. J. *17*, 10. https://doi.org/10.14806/ej.17.1.200.

64. Sedlazeck, F.J., Rescheneder, P., Smolka, M., Fang, H., Nattestad, M., von Haeseler, A., and Schatz, M.C. (2018). Accurate detection of complex structural variations using single-molecule sequencing. Nat. Methods *15*, 461–468. https://doi.org/10.1038/s41592-018-0001-7.

65. Ramírez, F., Bhardwaj, V., Arrigoni, L., Lam, K.C., Grüning, B.A., Villaveces, J., Habermann, B., Akhtar, A., and Manke, T. (2018). High-resolution TADs reveal DNA sequences underlying genome organization in flies. Nat. Commun. *9*, 189. https://doi.org/10.1038/s41467-017-02525-w.

66. Lopez-Delisle, L., Rabbani, L., Wolff, J., Bhardwaj, V., Backofen, R., Grüning, B., Ramírez, F., and Manke, T. (2021). pyGenomeTracks: reproducible plots for multivariate genomic datasets. Bioinformatics *37*, 422–423. https://doi.org/10.1093/bioinformatics/btaa692.

Supplemental Information

Genome editing in the mouse brain

with minimally immunogenic Cas9 RNPs

Elizabeth C. Stahl, Jennifer K. Sabo, Min Hyung Kang, Ryan Allen, Elizabeth Applegate, Shin Eui Kim, Yoonjin Kwon, Anmol Seth, Nicholas Lemus, Viviana Salinas-Rios, Katarzyna M. Soczek, Marena Trinidad, Linda T. Vo, Chris Jeans, Anna Wozniak, Timothy Morris, Athen Kimberlin, Thomas Foti, David F. Savage, and Jennifer A. Doudna

Table S1.

Primer sequences for NGS amplicon sequencing and ddPCR. All primers for Illumina MiSeq were ordered with (GCTCTTCCGATCT) at the 5' end for library preparation and indexing.

Primer Name	Sequence (5' → 3')	Assay/Application
BS-272 Forward	GCTCCTGGGCAACGTGCTGGTTATTG	tdTomato on-target (long read PacBio)
BS-273 Reverse	TTGATGACCTCCTCGCCCTTGCTCAC	tdTomato on-target (long read PacBio)
SauCas9 OT1 (chr2) Forward	GCACATGGACATGGATTTGTTCA	tdTomato off-target (short read Illumina MiSeq)
SauCas9 OT1 (chr2) Reverse	AGACCCACAAAGATCACAGGTAA	tdTomato off-target (short read Illumina MiSeq)
SauCas9 OT2 (chr18) Forward	TCATCTTTTGGGGGATTGCCT	tdTomato off-target (short read Illumina MiSeq)
SauCas9 OT2 (chr18) Reverse	AGGCCATTGTCCATGGAGTC	tdTomato off-target (short read Illumina MiSeq)
SauCas9 OT3 (chr1) Forward	CATGCTTACCACAGGCTCCA	tdTomato off-target (short read Illumina MiSeq)
SauCas9 OT3 (chr1) Reverse	ACTGTTACCCAGCCTCTCCT	tdTomato off-target (short read Illumina MiSeq)
SauCas9 OT4 (chr13) Forward	TTTAAGGACTTGGCAGACCACT	tdTomato off-target (short read Illumina MiSeq)
SauCas9 OT4 (chr13) Reverse	TGAGCGACCATGACCCTGTAA	tdTomato off-target (short read Illumina MiSeq)
SauCas9 OT5 (chr17) Forward	TGCCAACAGAAAAACCACAGC	tdTomato off-target (short read Illumina MiSeq)
SauCas9 OT5 (chr17) Reverse	AGCTTCCCTAAACCCAAGAGC	tdTomato off-target (short read Illumina MiSeq)
SauCas9 OT6 (chr4-1) Forward	TCACCCAGCAACTTGTGGAA	tdTomato off-target (short read Illumina MiSeq)
SauCas9 OT6 (chr4-1) Reverse	TAGGGATCCAAAAGCTGGGA	tdTomato off-target (short read Illumina MiSeq)
SauCas9 OT7 (chr4-2) Forward	GCAGAGCAGCAGGCATTCTT	tdTomato off-target (short read Illumina MiSeq)
SauCas9 OT7 (chr4-2) Reverse	AGGTTCACCCATTCTTGACTTCT	tdTomato off-target (short read Illumina MiSeq)
SauCas9 OT8 (chr9) Forward	TCAGAGACAACAATCCTAGCAGA	tdTomato off-target (short read Illumina MiSeq)
SauCas9 OT8 (chr9) Reverse	GGGCCTATCTGTCCTTGGGTA	tdTomato off-target (short read Illumina MiSeq)
SauCas9 OT9 (chrX-1) Forward	GGTTCCAAACCTCCCTAACAAC	tdTomato off-target (short read Illumina MiSeq)
SauCas9 OT9 (chrX-1) Reverse	ATGTCATCCCTAGTTCCTATGTAAA	tdTomato off-target (short read Illumina MiSeq)
SauCas9 OT10 (chrX-2) Forward	CCCTGGGCTTAGCCATTTCT	tdTomato off-target (short read Illumina MiSeq)

SauCas9 OT10 (chrX-2) Reverse	CCCACAACCCTAGTTGAGCC	tdTomato off-target (short read Illumina MiSeq)
SpyCas9 OT1 (chr4-3) Forward	CTGGTTCCCACTGGACCTTC	tdTomato off-target (short read Illumina MiSeq)
SpyCas9 OT1 (chr4-3) Reverse	GCCATGGTGTGTAAAGTAGGTG	tdTomato off-target (short read Illumina MiSeq)
SpyCas9 OT2 (chr17-2) Forward	ATCCATGTTGGGGGTTTAGTT	tdTomato off-target (short read Illumina MiSeq)
SpyCas9 OT2 (chr17-2) Reverse	GGGGGACTTTTGGGATAGCA	tdTomato off-target (short read Illumina MiSeq)
SpyCas9 OT3 (chr12) Forward	CCACATTCCCATCCCCAGAA	tdTomato off-target (short read Illumina MiSeq)
SpyCas9 OT3 (chr12) Reverse	CAGTTTTGCTAGGGGGAGTG	tdTomato off-target (short read Illumina MiSeq)
SpyCas9 OT4 (chr15) Forward	CACCAGGACCTCTATGGTGC	tdTomato off-target (short read Illumina MiSeq)
SpyCas9 OT4 (chr15) Reverse	GCTCCTGCTAGGAGGTATTTGG	tdTomato off-target (short read Illumina MiSeq)
SpyCas9 OT5 (chr19) Forward	GGTGCCTCTAAGCATCCTGAAT	tdTomato off-target (short read Illumina MiSeq)
SpyCas9 OT5 (chr19) Reverse	AAGTAGCTGGCATGTTCGGT	tdTomato off-target (short read Illumina MiSeq)
SauCas9 Forward	GGAAGAGAAATACGTGGCCG	ddPCR cDNA (gene expression)
SauCas9 Reverse	GGCTTCTTTCACGTAGTCGC	ddPCR cDNA (gene expression)
SauCas9 probe (FAM)	AGAAAGACGGCGAAGTGCGG	ddPCR cDNA (gene expression)
EMX1 Forward	GTGTGGTTCCAGAACCGGA	EMX1 on-target (short read Illumina MiSeq)
EMX1 Reverse	GCCTGCTTCGTGGCAATG	EMX1 on-target (short read Illumina MiSeq)

Table S2.

Assay IDs for qPCR and ddPCR assays.

Gene Symbol	Assay Catalog #	Manufacturer	Assay/Application
Rbfox3	PPM60749A	Qiagen	qPCR
Gfap	PPM04716A	Qiagen	qPCR
Aif1	PPM03752A	Qiagen	qPCR
Itgam	PPM03671F	Qiagen	qPCR
Cd19	PPM03218A	Qiagen	qPCR
Sdc1	PPM03216A	Qiagen	qPCR
Cd3e	PPM04598A	Qiagen	qPCR
Cd4	PPM04028F	Qiagen	qPCR
Cd8a	PPM04031A	Qiagen	qPCR
Il2	PPM02937C	Qiagen	qPCR
Il2ra	PPM03125C	Qiagen	qPCR
Il10	PPM03017C	Qiagen	qPCR
Tnf	PPM03113G	Qiagen	qPCR
Il1b	PPM03109F	Qiagen	qPCR
Ifng	PPM03121A	Qiagen	qPCR
Fas	PPM03705B	Qiagen	qPCR
Fasl	PPM02926E	Qiagen	qPCR
Nfkb1	PPM02930F	Qiagen	qPCR
Il6	PPM03015A	Qiagen	qPCR
Ppih	PPM03699A	Qiagen	qPCR
Gapdh	PPM02946E	Qiagen	qPCR
MGDC (control)	PPM65836A	Qiagen	qPCR
RTC (control)	PPX63340A	Qiagen	qPCR
PPC (control)	PPX63339A	Qiagen	qPCR
Cdkn1a, 4930567H12Rik	Mm04205640_g1	ThermoFisher	qPCR
Gapdh	Mm99999915_g1	ThermoFisher	qPCR
SpyCas9 NHEJ	dMmuNHS102024435	Bio-Rad	ddPCR (includes primers and probes (HEX, FAM))
SauCas9 NHEJ	dMmuNHS228153217	Bio-Rad	ddPCR (includes primers and probes (HEX, FAM))

Table S3.

Off-targets predicted by Cas-OFFinder for SauCas9 (spo4 spacer: 5'
TCCAGACATGATAAGATACATTG) evaluated in this study.

OT	Mismatches	Bulge (Type)	Chromosome (GRCm39)	Sequences (5'→ 3' NNGRRT PAM)
1	2	2 (RNA)	Chr2	TCCAG—ATGtTAAGATACATTa TAGAGT TCCAGA—TGtTAAGATACATTa TAGAGT
2	2	2 (RNA)	Chr18	TCCAG—ATaATAAaATACATTG AGGAGT TCCAGA—TaATAAaATACATTG AGGAGT TCCAGAtA—ATAAaATACATTG AGGAGT
3	3	1 (RNA)	Chr1	TCCtGACATG-TAAGATgCtTTG AGGGGT
4	3	1 (DNA)	Chr13	TCaAGACAaGTATAAaATACATTG GTGGGT
5	3	1 (DNA)	Chr17	TCaAGACAaGTtTAAGATACATTG GTGGAT TCaAGACAaGtTTAAGATACATTG GTGGAT TCaAGACAaGtTTAAGATACATTG GTGGAT
6	3	1 (DNA)	Chr4	TCACAGACATtATAAGAaACATTa CAGAAT
7	3	1 (RNA)	Chr4	TCCAtACAT-ATAAGATAgATgG ATGGAT
8	3	1 (RNA)	Chr9	TCCAaAaATGATcAGATAC-TTG GTGAAT
9	3	1 (RNA)	ChrX	T-CAGAaATaAgAAGATACATTG CAGAGT TC-AGAaATaAgAAGATACATTG CAGAGT
10	3	1 (RNA)	ChrX	TCCAGAC-TcATAAGATACAggG CAGGAT

Table S4.

Off-targets predicted by Cas-OFFinder for SpyCas9 (sg298 spacer: 5'
AAGTAAAACCTCTACAAATG) evaluated in this study.

OT	Mismatches	Bulge (Type)	Chromosome (GRCm39)	Sequences (5'→ 3' NGG PAM)
1	3	0	Chr4	AAtTAgAACCTCTACAgATG AGG
2	3	0	Chr12	AAGTAAAACCTCaACAgAaG GGG
3	3	0	Chr15	AAGTAAAACCTCTACcAAaa GGG
4	3	0	Chr17	AAGTAtgACCTaTACAAATG GGG
5	3	0	Chr19	AAtTAAAAgCTCTACAAAaG GGG

A

SpyCas9 spacer (PAM): 5' AAGTAAAACCTCTACAAATG (TGG), antisense
SauCas9 spacer (PAM): 5' TCCAGACATGATAAGATACATTG (ATGAGT), antisense

B

C

D

E

Mouse NPCs
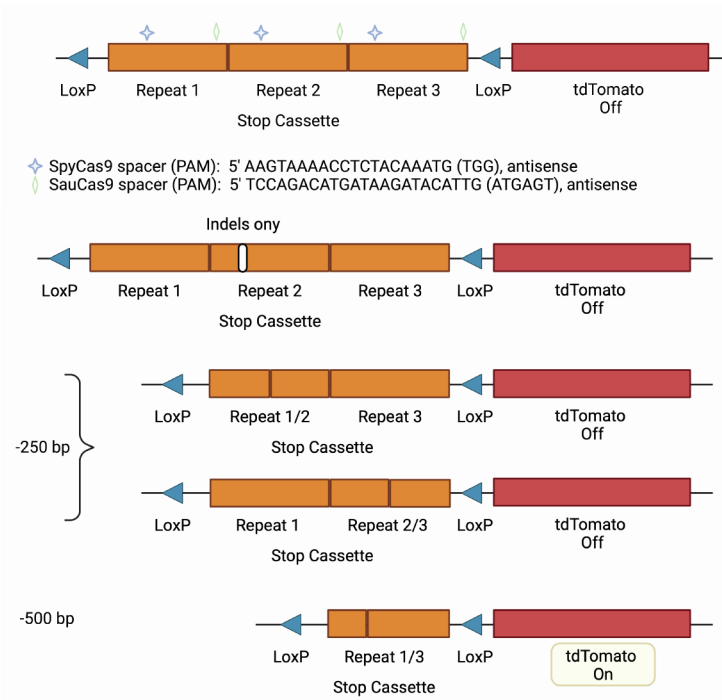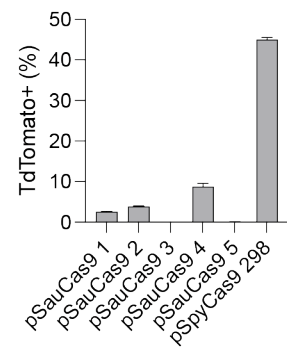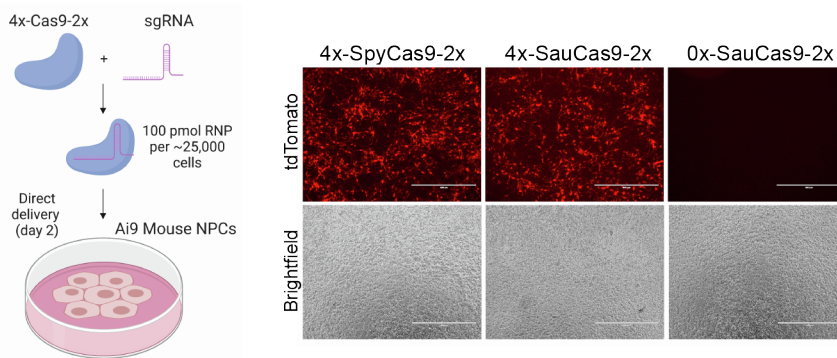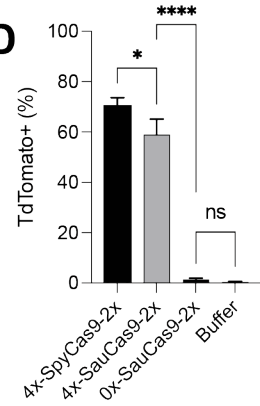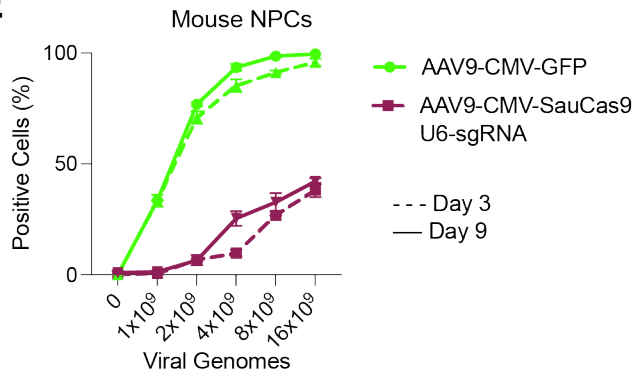
F
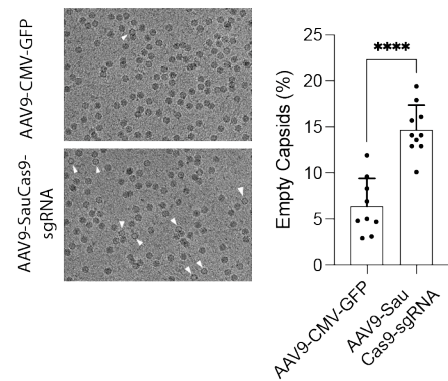
Figure S1. Adapting tdTomato reporter system for SauCas9 genome editing with RNPs and AAVs in vitro.

A) Schematic of tdTomato locus in Ai9 mice, created with Biorender.com. Three stop repeats are flanked by LoxP sites upstream of the tdTomato reporter, which separates tdTomato from its promoter within the Rosa26 locus. The relative target sites for SpyCas9 (sg298) and SauCas9 (spacer4) are shown including the spacer and PAM sequences. After dsDNA breaks, there can be several editing outcomes, including indels only in any of the three repeats (one shown here), deletions of approximately 250bp from neighboring repeats, or large deletions of approximately 500bp from distal repeats, which is the only outcome sufficient to turn on the tdTomato reporter. Therefore, tdTomato fluorescent signal is an underestimate of total editing events.

B) Flow cytometry results from vitro experiment for SauCas9 tdTomato guide selection. Neural precursor cells (NPCs) from E13.5 Ai9 mice were transfected with six plasmids: five plasmids encoded SauCas9 with five different spacer sequences and one plasmid encoded SpyCas9 with sg298 as a positive control. Puromycin selection was not performed. Out of the five SauCas9 guides, "spacer 4" performed the best and was selected for further study.

C) Schematic of RNP formation and direct delivery in Ai9 tdTomato mouse NPCs, created with BioRender.com. Representative fluorescent micrographs showing tdTomato signal in mouse NPCs five-days after treatment with RNPs prior to flow cytometry. Scale bar: 400μm.

D) Flow cytometry results from in vitro experiment testing cell entry and editing with 4x-SauCas9-2x RNP. Editing was measured by tdTomato expression after cell penetrant Cas9 RNPs were added to mouse neural precursor cells (NPCs) via "direct delivery" into the cell culture supernatant (100pmol, final 1uM concentration). Treatments were performed in triplicate and statistical significance was measured by one-way ANOVA with multiple comparisons (**** $p<0.001$, * $p<0.05$, ns = not significant).

E) Flow cytometry results after viral transduction of mouse NPCs with a virus encoding the GFP transgene neared 100% when 10,000 cells received 2e9 viral genomes (vg), while editing as measured by tdTomato expression reached a maximum of approx. 40% at the highest tested dose of 16e9 vg. Above 8e9 vg, cell viability was visibly decreased.

F) Cryo-electron microscopy of AAV9 capsids. Three individuals blinded to the identify of 9-10 images per group counted empty (arrows) versus full capsids in ImageJ. The three counts per image were averaged then plotted between the two groups (student's t-test, **** $p<0.001$).
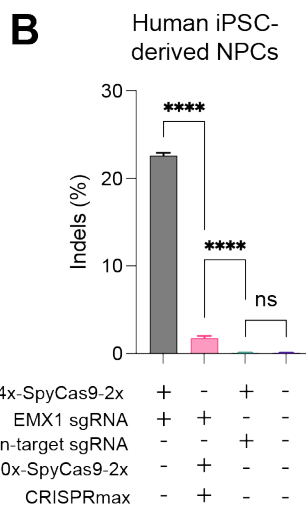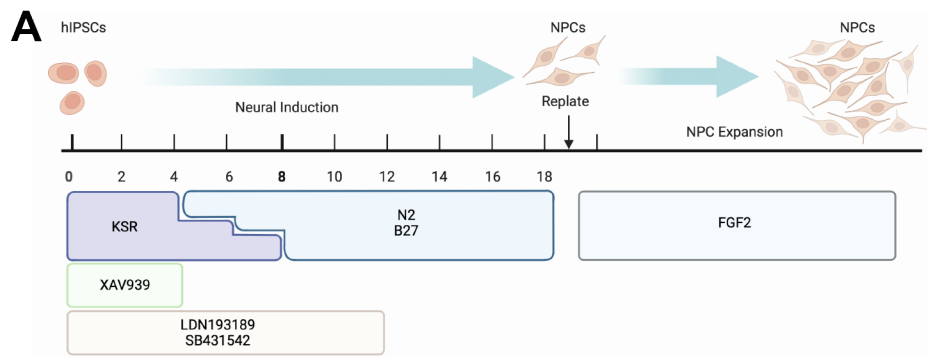
Figure S2. Direct delivery of 4xNLS-Cas9 RNPs results in significant editing of primary human NPCs.

A) Schmatic of human induced pluripotent stem cell (iPSC) differentiation into neural precursor cells (NPCs) and expansion. Created with Biorender.com.

B) Quantification of editing of EMX1 locus in iPSC-derived NPCs (n=3 replicates, one-way ANOVA, ****p<0.001). CRISPRmax was incubated with non-cell-penetrating 0x-SpyCas9-2x RNPs to aid cell entry, according to the manufacturer's instructions, and editing was compared to 4x-SpyCas9-2x RNPs alone.

A Intrathecal Injection

Sham   4x-SpyCas9-2x

tdTomato / DAPI
NeuN   S100β   DARPP-32

4x-SpyCas9-2x
Striatum
Cortex

B Intracerebroventricular (neonatal p0)

Sham   4x-SpyCas9-2x

S100β   tdTomato   S100β /tdTomato/ DAPI
SVZ

OLIG2   tdTomato   Merge
White Matter

C

Ki67 /tdTomato/ DAPI   DCX /tdTomato/ DAPI
SVZ

D Intracerebroventricular (adult)

tdTomato / DAPI

E Intracerebroventricular (adult)

SVZ

Hippocampus

tdTomato   tdTomato / DAPI

F

ICV
-0.7mm A/P

Intrastriatal
+0.7 mm A/P

— RNP Intrastriatal (n=5)
— RNP ICV (n=10)

TdTomato⁺ Cells

Distance from Bregma (mm)

9

Figure S3. Intrathecal and intracerebroventricular (ICV) administration of Cas9 RNPs.

A) Intrathecal injection of 300μM 4x-SpyCas9-2x into the sub-arachnoid space in adult Ai9 mice analyzed 21-days post-injection. Edited NeuN+ neurons and S100beta+ glial cells were detected in the cortex and striatum of one mouse, including DARPP-32 medium spiny neurons. Only 1 of 3 mice at the 300μM dose showed tdTomato signal in the brain. Additional mice that received intrathecal injection of RNP at 100μM (n=4), 200μM (n=4), and 400μM (n=5) did not have detectable editing in the brain or spinal cord.

B) ICV injection of 100μM 4x-SpyCas9-2x into the lateral ventricle of neonatal p0 mice analyzed 21-days post-injection. Edited S100beta+ and OLIG2+ glial cells were identified in the subventricular zone (SVZ) and white matter. Representative image shown (n=1 of 5). All 5 injected mice had similar levels of editing, however, some also showed signs of ventriculomegaly.

C) ICV injection of p0 mice also led to tdTomato expression (editing) in neural stem/progenitor cells that express Ki67 and DCX.

D) ICV injection of adult mice with 100-400μM 4x-SpyCas9-2x led to edited tdTomato+ cells in the SVZ, choiroid plexus, ventricle, corpus callosum, and hippocampus (images shown from 3 different biological replicates).

E) Zoomed (20x magnification) image of tiled slide scan of adult ICV injection in two replicates showing tdTomato+ cells in hippocampus and sub-ventricular zone (SVZ). Scale bar: 100μm.

F) Quantification of tdTomato+ cells in adult Ai9 mice for ICV route versus intrastriatal injections. From n=5 injections, the intrastriatal route resulted in an average of 3631 tdTomato+ cells per striatum (range 1943 to 6209). From n=10 injections, all 10 mice had tdTomato signal in the tissue near the ventricles, averaging 859 tdTomato+ cells per brain (range 295 to 4329), demonstrating direct injection of RNP is most effective for editing in the mouse brain.
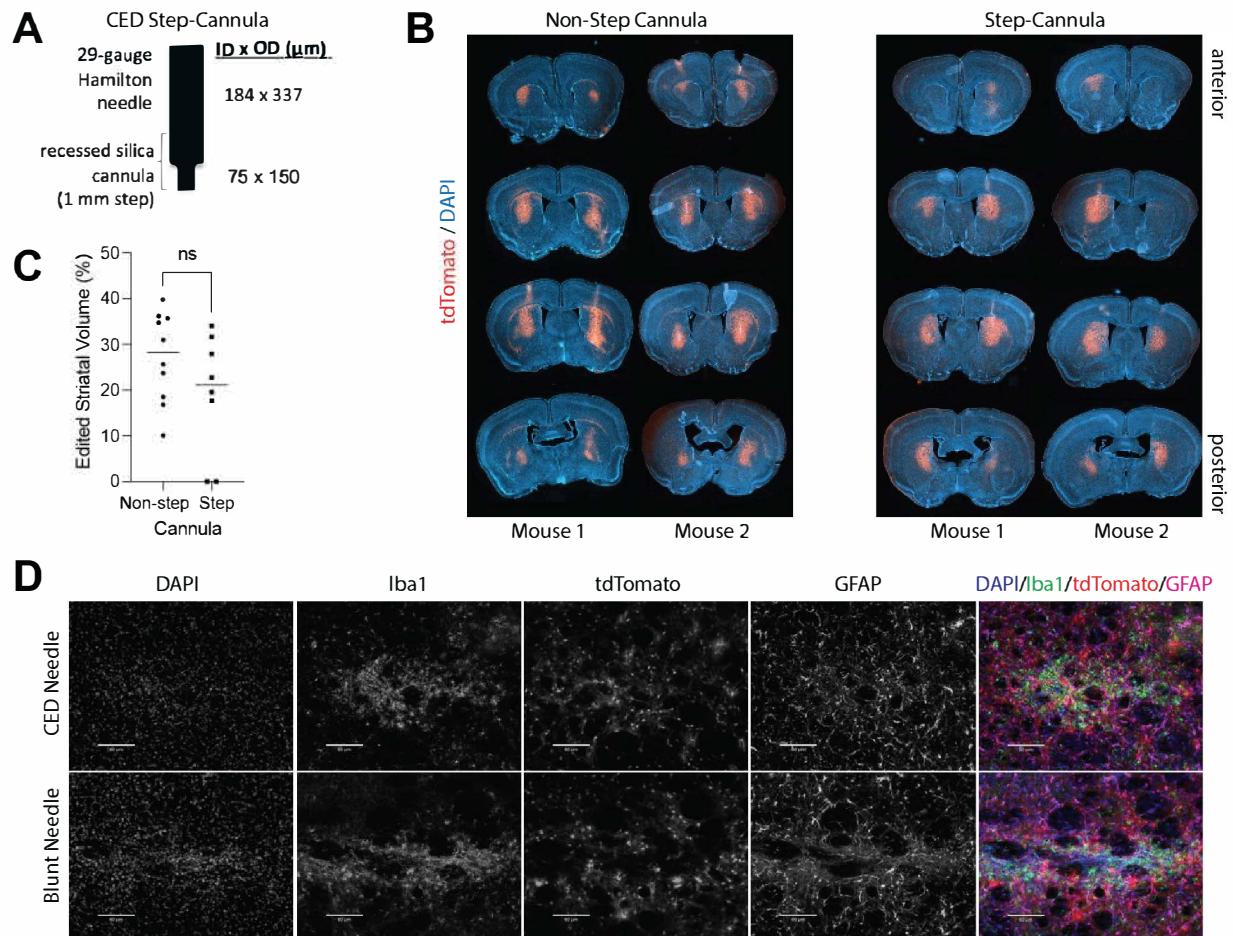
Figure S4. Convection enhanced delivery of RNPs.

A) Schematic of convection enhanced delivery (CED) needle with step-cannula.

B) Representative images of two biological replicates of intrastriatal bilateral injections of 4x-SpyCas9-2x RNP at 25µM (125pmol) per hemisphere at 7-days post-injection.

C) Quantification of edited striatal volume in the non-step cannula (n=10 techncial replicates) and the step-cannula (n=8 technical replicates) showed no signficiant difference. Of note, the step-cannula group contained two failed injections (along x-axis). Additionally, two mice did not recover from surgery in the step-cannula group and one mouse did not recover from surgery in the non-step cannula group (data not shown).

D) Representative images of Iba1 and GFAP staining near the injeciton site in the striatum demonstrated similar levels of microglial and glial cell reaction between the step and non-step cannulas. Scale bar: 50µm.

A

	Theoretical Charge	Elution KCl (mM)
0x-SpyCas9-2x	+ 30	470
4x-SpyCas9-2x	+ 50	690
0x-SauCas9-2x	+ 40	660
4x-SauCas9-2x	+ 61	760
3x-SauCas9-2x	+ 56	730
2x-SauCas9-2x	+ 51	700

B

1. 4xNLS   126.4 kDa
2. 3xNLS   125.4 kDa
3. 2xNLS   123.4 kDa
4. Markers

C

Nucleofection

Direct Delivery

D   25μM

Sham   4x-SpyCas9-2x   2x-SauCas9-2x   3x-SauCas9-2x   4x-SauCas9-2x

E   100μM 4x-SauCas9-2x

F

DAPI   tdTomato

10x

40x

NeuN   GFAP   tdTomato/NeuN   tdTomato/GFAP

G   Dynamic Light Scattering (DLS)

4x-SpyCas9-2x   4x-SauCas9-2x

25C 30 mins

37C 30 mins

12
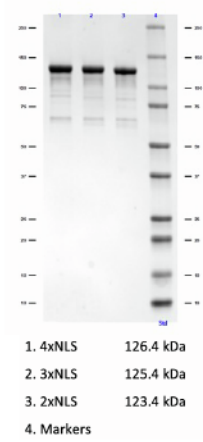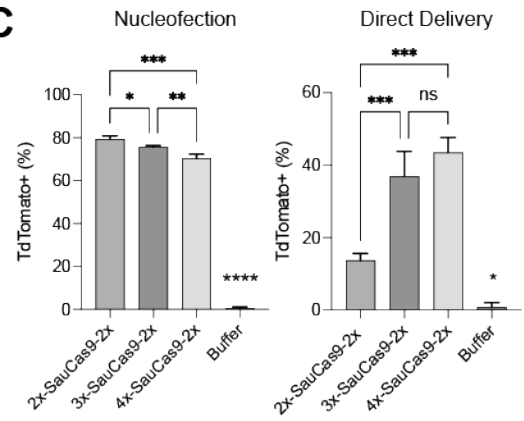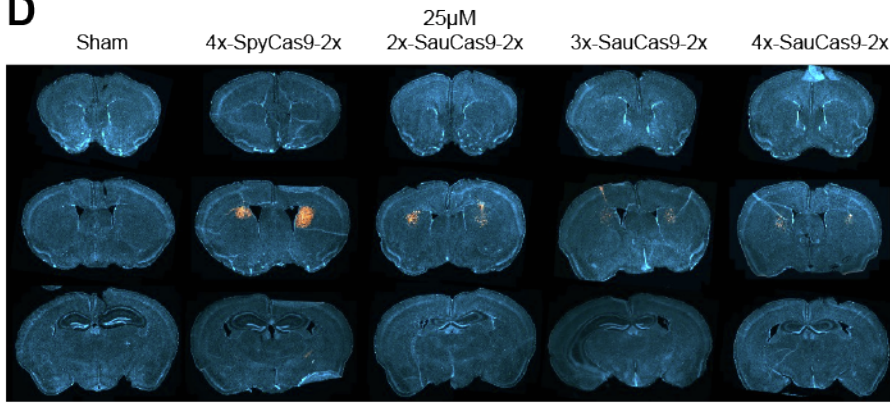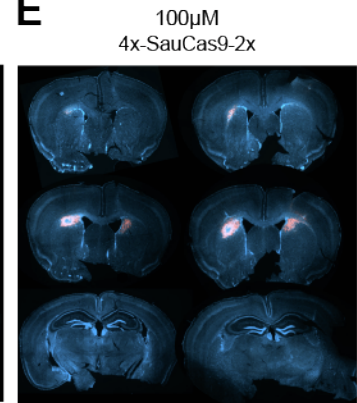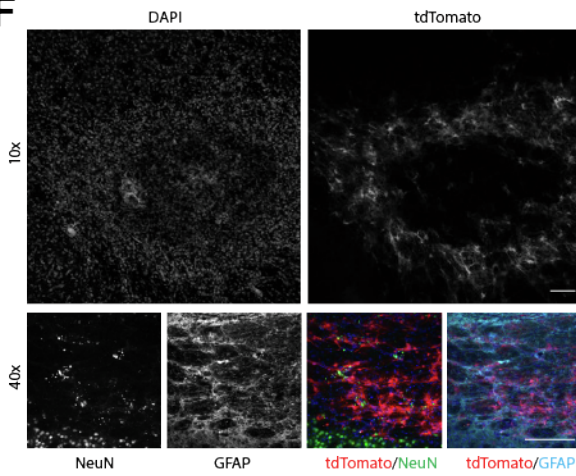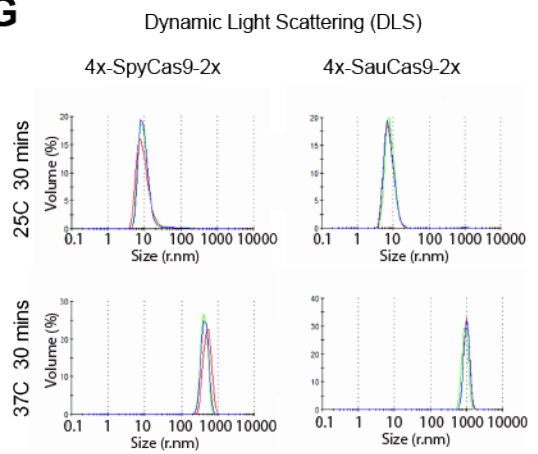
Figure S5. Optimizing SauCas9 RNP NLS structure for self-delivery in vivo.

A) Theoretical charge and measured elution concentration of SpyCas9 and SauCas9 variants with different SV40 NLS architectures on the N and C terminus.

B) SDS-PAGE gel showing the expression purity and size of the three SauCas9 NLS variants.

C) Flow cytometry results of editing in Ai9 NPCs from three SauCas9 variants with 2, 3, and 4 copies of SV40 NLS on the N-terminus. The 4x-SauCas9-2x variant was most effective at direct entry into the cell (added to cell culture supernatant at 100pmol, 1µM final concentration, 48-hours after seeding the cells), however the 2x-SauCas9-2x variant was most effective at editing the cells when nucleofected, suggesting the NLS can interfere with editing function but enhances cell-entry.

D) Representative images (1 of 2 biological replicates shown) of bilateral intrastriatal injection of RNPs (25uM, 125 pmol dose) analyzed at 21-days shows very limited editing with SauCas9 RNPs in vivo. All groups lagged behind 4x-SpyCas9-2x RNP at in vivo efficiency (20µm thick OCT-embedded sections).

E) Representative images (2 of 3 biological replicates) of bilateral intrastriatal injection of RNPs (100µM, 500 pmol dose) analyzed at 21-days shows very limited editing with SauCas9 RNPs in vivo (50µm thick agarose embedded sections).

F) Confocal images of edited striatum in 4x-SauCas9-2x RNP group 21-days after injection at 500pmol. The tdTomato often had a "donut shape" pattern where signal was lost from the center, concomitant with loss of NeuN and enhanced GFAP staining, suggesting dose-limiting toxicity. 10x images and 40x images were imaged on different days and reflect the same group, but not the same section. Scale bar: 100 µm.

G) Dynamic light scattering experiment with Cas9 RNPs incubated at 25 or 37C showing increase in size distribution by mass peak over time. Larger RNPs could indicate aggregation, likely following temperature-induced protein misfolding.
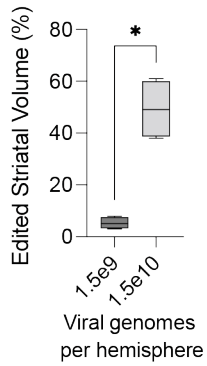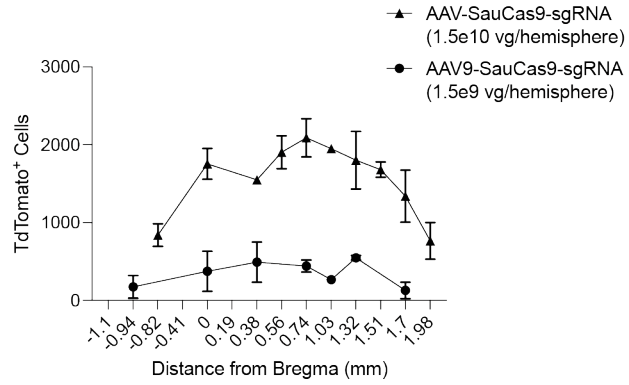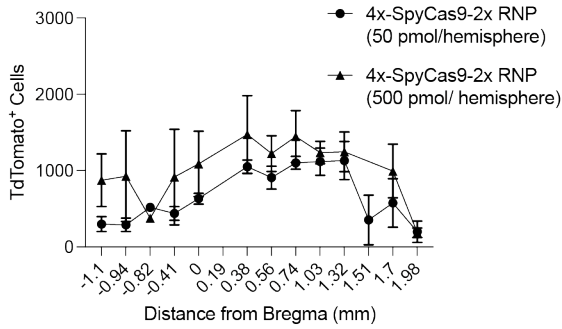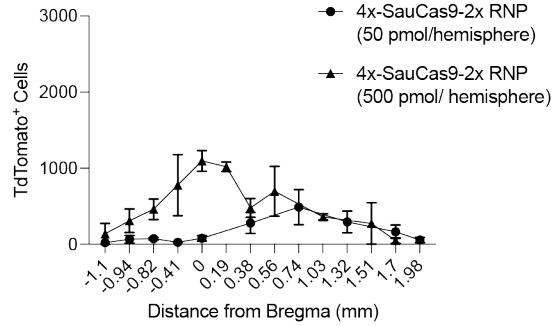
14
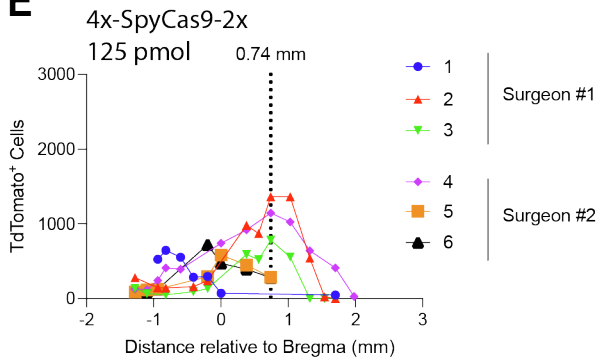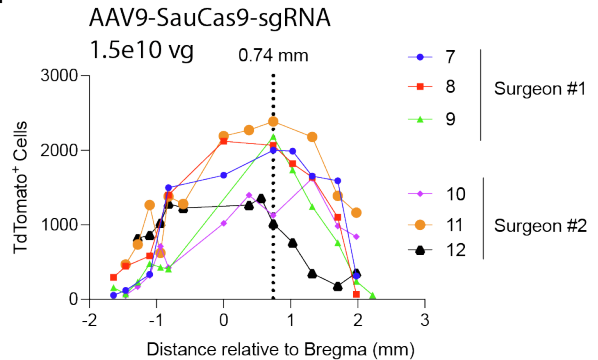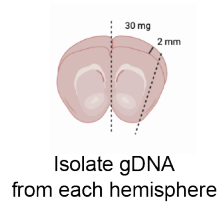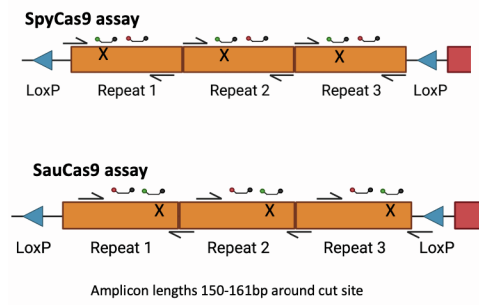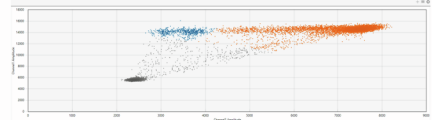
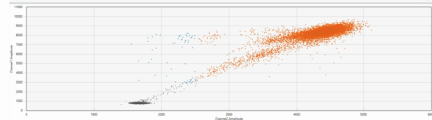**Figure S6. Dose dependent effects on distribution of Cas9-AAV and Cas9-RNPs in the brain.**

A) Edited tissue volume calculated as a percentage of total striatum (%) for AAV9-CMV-SauCas9-U6-sgRNA injected at 3e8 vg/μL and 3e9 vg/μL (1.5e9-1.5e10 vg/hemisphere) analyzed at 90-days post-injection. Unpaired t-test, *p<0.05.

B) Total tdTomato+ cell counts per hemisphere (all brain regions) along the rostral-caudal axis for AAV9-CMV-SauCas9-U6-sgRNA injected at 3e8 vg/μL and 3e9 vg/μL (1.5e9-1.5e10 vg/hemisphere) analyzed at 90-days post-injection. Mean +/- standard error (n=4 injections).

C) Total tdTomato+ cell counts per hemisphere (all brain regions) along the rostral-caudal axis for 4x-SpyCas9-2x RNPs at 50 or 500 pmol dose analyzed up to 90-days post-injection. Mean +/- standard error (n=4 injections).

D) Total tdTomato+ cell counts per hemisphere (all brain regions) along the rostral-caudal axis for 4x-SauCas9-2x RNPs at 50 or 500 pmol dose analyzed up to 90-days post-injection. Mean +/- standard error (n=4 injections).

E) Individual replicates of total tdTomato+ cell counts per hemisphere (all brain regions) of mice that received injections of 4x-SpyCas9-2x analyzed at 21-days. Cas9 RNPs (25μM, 125pmol, n=6) had a maximum number of 1000 edited cells near the injection site (dotted line 0.74 mm relative to Bregma).

F) Individual replicates of total tdTomato+ cell counts per hemisphere (all brain regions) of mice injected with AAV9-CMV-SauCas9-U6-sgRNA analyzed at 21-days. Cas9 AAVs (3e9 vg/μL,1.5e10 vg/hemisphere, n=6) resulted in a maximum of 2000 edited cells near the injection site and diffused more broadly along the anterior-posterior axis.

A

30 mg
2 mm

Isolate gDNA
from each hemisphere

B

SpyCas9 assay

LoxP   Repeat 1   Repeat 2   Repeat 3   LoxP

SauCas9 assay

LoxP   Repeat 1   Repeat 2   Repeat 3   LoxP

Amplicon lengths 150-161bp around cut site

C

Example AAV-SauCas9-sgRNA with automated gating strategy (sample 71-4R, 19.94%)

Example SpyCas9 RNP with automated gating strategy (sample 71-5R, 1.53%)

Example Sham with automated gating strategy (sample 71-1R, 0%)

D

SauCas9
ddPCR Assay

Fractional Abundance
(indels, %)

20
15
10
5
0.3
0.2
0.1
0.0

3 dpi   14 dpi   28 dpi

● AAV9-SauCsa9-sgRNA
(1.5e10 vg/hemisphere)
● 4x-SauCas9-2x RNP
(125 pmol / hemisphere)
● Sham

SpyCas9
ddPCR Assay

(indels, %)

2.5
2.0
1.5
1.0
0.5
0.0

3 dpi   14 dpi   28 dpi
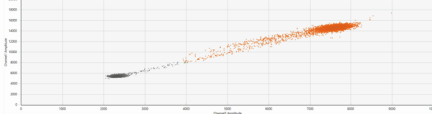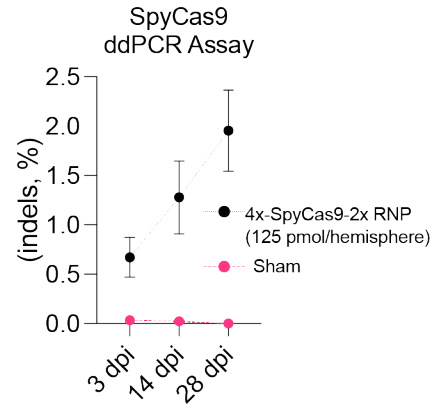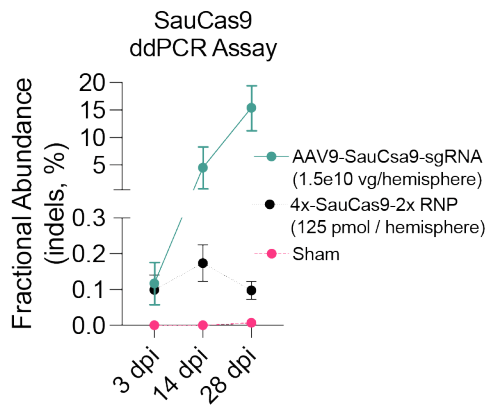
● 4x-SpyCas9-2x RNP
(125 pmol/hemisphere)
● Sham

16

Figure S7. Development of ddPCR assay for editing outcomes with SpyCas9-sg298 and SauCas9-spacer4 at tdTomato locus.

A) Schematic of tissue collection. Approximately 30 mg of brain tissue (2 mm thick) was isolated from one hemisphere of the mouse striatum, encompassing the intended injection site. Tissue was flash frozen and later processed for genomic DNA (gDNA). Image made using Biorender.com.

B) Schematic of PCR products, approximately 160bp around the three stop repeats containing the cut site. Two probes bind to the amplicon. The FAM-labeled probe is the reference, while the HEX-labeled probe sits directly over the intended cut-site and will be lost due to indels or large deletions. Due to different gRNA requirements, each ortholog was assessed with a different primer/probe set. If FAM and HEX intensity are proportional in a single droplet, then no editing is detected, whereas a droplet that loses HEX in greater proportion to FAM would indicate an editing event.

C) Representative results showing FAM$^+$ / HEX$^-$ population (blue) in Cas9-AAV, RNP, and sham injected mice, signifying disruption of the tdTomato locus.

D) Quantification of digital droplet PCR (ddPCR) assays show detectable editing in AAV9-SauCas9-sgRNA, 4x- SauCas9-2x NLS, and 4x-SpyCas9-2x groups (25µM, 125pmol, n=6 technical replicates) in 30mg tissue hemispheres (2-mm thick) above background (sham).

A

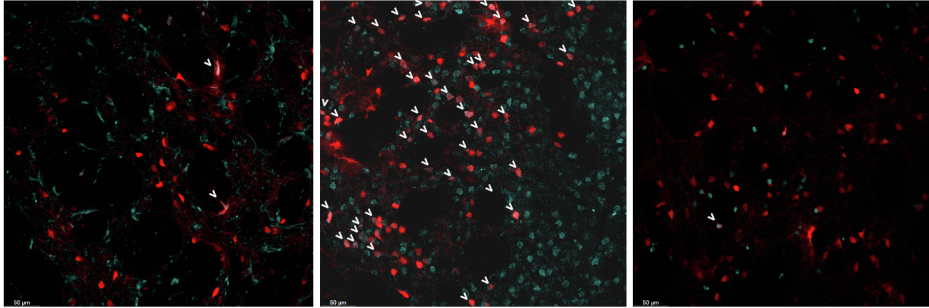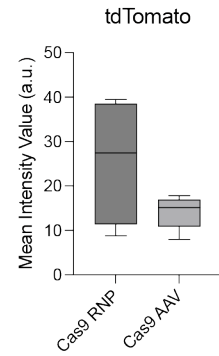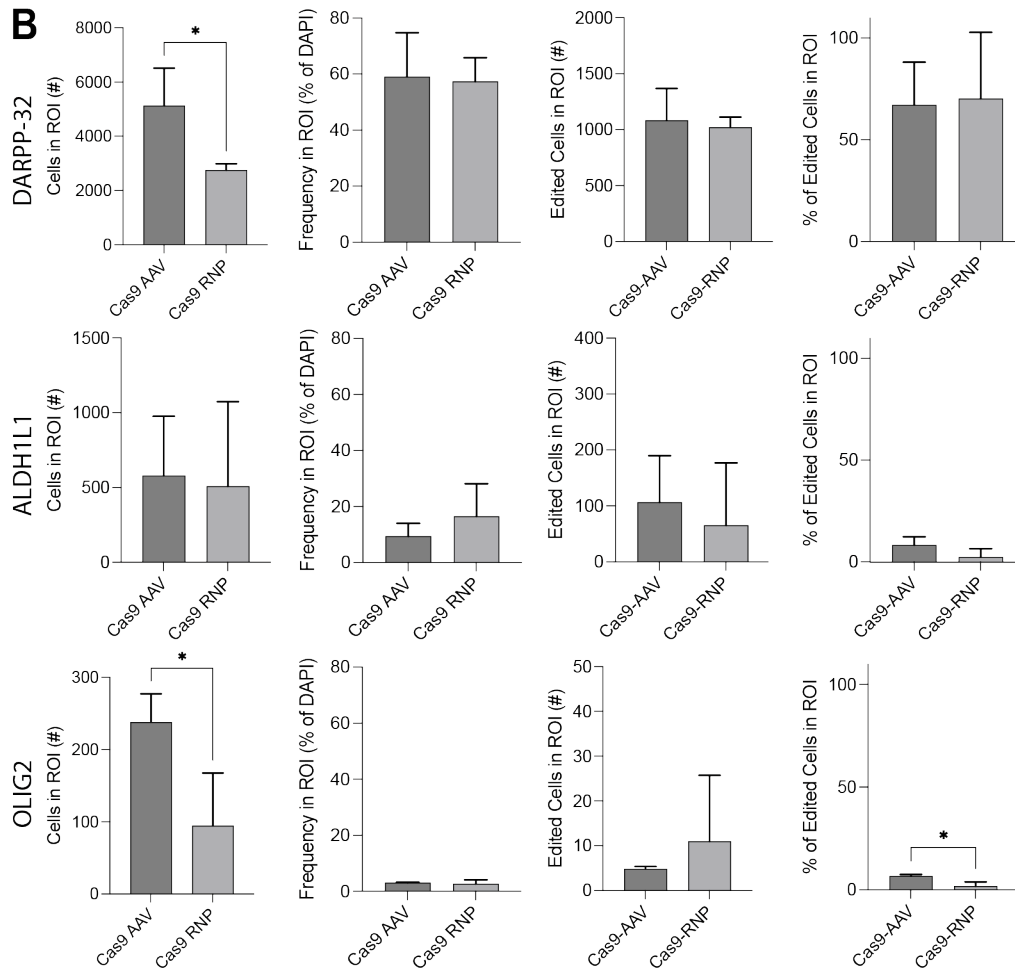tdTomato / ALDH1L1   tdTomato / DARPP-32   tdTomato / OLIG2

Cas9 RNP

C

tdTomato

B

Figure S8. Edited Cell Distribution and tdTomato intensity.

A) Representative images of ALDH1L1, DARPP-32, and OLIG2 immunostaining staining (cyan) with tdTomato (red) in the mouse hippocampus 21-days post-delivery of Cas9 RNPs (25μM). Arrows indicate cells co-expressing tdTomato and each cell marker. Scale bar: 50 μm.

B) Quantification of cell type editing for DARPP-32 (medium spiny neurons), ALDH1L1 (astrocytes), and OLIG2 (oligodendrocytes). Graphs in the first column show the total number of cells expressing the indicated marker within the region of interest (ROI). ROIs were often larger for Cas9-AAV due to greater lateral diffusion and thus contain more cells (n=3 injections, unpaired t-test, * $p<0.05$). The second column shows the frequency of each cell type in the ROI as a percentage of total cells. There was no significant difference in the frequency of each cell type within the ROI (i.e., no population death or expansion in response to treatment), although there was a trend towards more ALDH1L1$^+$ cells in the Cas9 RNP group. Column 3 shows the number of edited (tdTomato$^+$) cells within the ROI expressing the given marker. Despite larger ROIs, there was no significant increase in edited cell counts in the Cas9 RNP group. The fourth column shows the frequency of edited cells within the ROI. In both Cas9 AAV and RNP, edited DARPP-32$^+$ cells accounted for greater than half of the total edited cells. The DARPP-32 data complements the NeuN data in Figure 1J, demonstrating that Cas9 RNPs result in the same or more edited neurons than Cas9 AAVs within a given area. Glial cells accounted for a significantly greater proportion of total edited cells in the Cas9 AAV group compared to the Cas9 RNP group (* $p<0.05$).

C) Per cell mean intensity values of tdTomato were quantified within the ROIs for Cas9 AAV and RNPs. The tdTomato signal was often brighter in the Cas9 RNP group but was not statistically different (n=4-6 injections, unpaired t-test, ns). This observation could perhaps be due to differences in guide RNA editing outcomes or a greater frequency of biallelic editing in the Cas9-RNP group as tdTomato signal on requires two simultaneous cuts. Cas expression from AAV genome likely has a greater lag time to produce multiple Cas9 molecules required for gene excision and could thus lead to greater number of indels not captured by fluorescence measurements.
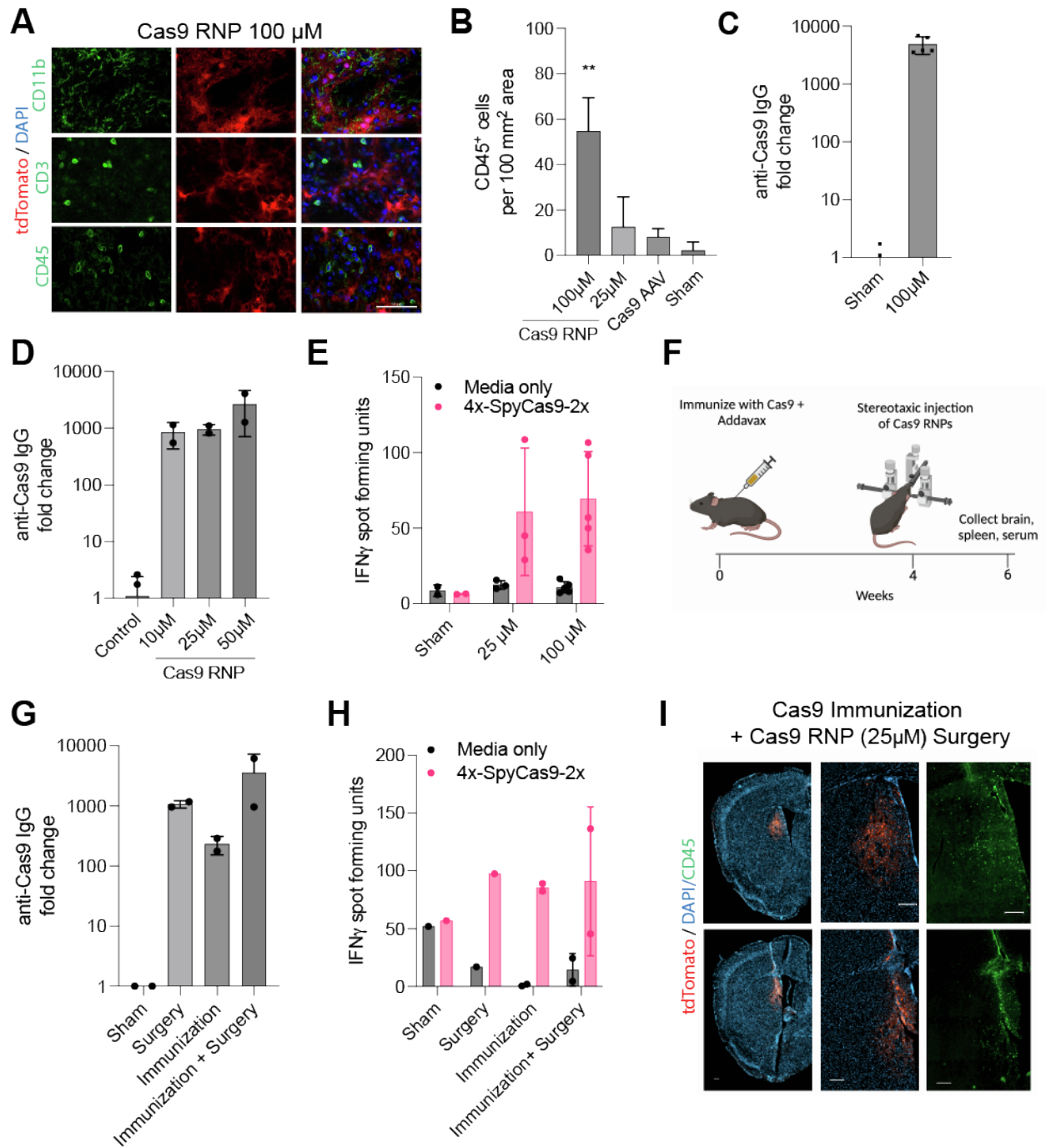
A Cas9 RNP 100 µM

B

C

D

E

F

G

H

I Cas9 Immunization + Cas9 RNP (25µM) Surgery

Figure S9. Cellular and humoral response to Cas9 RNPs at additional doses and following immunization with Addavax with Cas9 protein.

A) Representative staining of CD45, CD3, and CD11b in the Cas9 RNP 500pmol dose at 21-days. Scale bar: 50μm.

B) Quantification of CD45 immune cells at 21-days in Cas9 RNP 100 μM (500 pmol) dose compared to Cas9 RNP 25 μM (125 pmol), Cas9 AAV, and sham (as shown in Figure 3C, one-way ANOVA, ** $p < 0.01$).

C) Anti-Cas9 IgG measured by ELISA from serum collected 21-days post-treatment with Cas9 RNP 100 μM dose had similar fold change as the Cas9 RNP 25 μM dose (Figure 3E).

D) Anti-Cas9 IgG measured by ELISA from serum collected 90-days post-treatment with Cas9 RNP at 10 μM, 25 μM, and 100 μM doses.

E) Anti-Cas9 cellular response (interferon-gamma spot forming units) measured by ELISpot from splenocytes collected 21-days post-treatment with Cas9 RNP at 25 μM and100 μM compared to sham mice, restimulated in culture for 48 hours with media only or 4x-SpyCas9-2x.

F) Schematic of immunization strategy (25μg 4x-SpyCas9-2x injected subcutaneously with AddaVax, followed by stereotaxic surgery with 25 μM (10μL at 4.15 μg/μL: 41.5 μg) 4x-SpyCas9-2x). Created with Biorender.com.

G) Anti-Cas9 IgG measured by ELISA from serum collected 6-weeks post-immunization (2 weeks post-surgery if applicable). Sham mice received Addavax alone and no surgery, immunized mice received Addavax with 4x-SpyCas9-2x protein subcutaneously only, and surgery mice received25 μM 4x-SpyCas9-2x RNP into the striatum.

H) Anti-Cas9 cellular response (interferon-gamma spot forming units) measured by ELISpot from splenocytes collected 6 weeks post-immunization (2 weeks post-surgery if applicable).

I) Representative image of tdTomato editioning in the brain at 6 weeks post-immunization (2 weeks post-surgery) in a mouse that received both immunization and surgery. Many CD45^{+} cells were observed near tdTomato^{+} cells and along needle injection track, which resembled the response to higher doses of Cas9-RNPs. Edited cells persisted to the latest measured time point of 2-weeks. Scale bar: 200 μm.

A

1 month

Sham
SauCas9 RNP
SauCas9 AAV

Indels (%)

Predicted off-targets: chr2, chr18, chr1, chr13, chr17, chr4-1, chr4-2

B

Sham
SpyCas9 RNP

Indels (%)

Predicted off-targets: chr4-3, chr17-2, chr12, chr15, chr19

C

4 months

Sham
SauCas9 AAV

Indels (%)

Predicted off-targets: chr2, chr18, chr1, chr13, chr17, chr4-1, chr4-2, chr9, chrX-1, chrX-2

D

4 months

SauCas9 expression (copies / ng RNA)
Indels (%)

16R, 17R, 18R, 18L — Sham
22R, 22L, 24R, 24L — AAV-SauCas9-sgRNA
19L, 20L, 21R, 21L — 4x-SauCas9-2x RNP
14R, 14L, 15R, 15L — 4x-SpyCas9-2x RNP

E

Cdkn1a (p21)
28-days

RT-qPCR
Fold Change

Sham 1.03
Cas9 RNP 0.98
Cas9 AAV 1.27

F

4 months

Rbfox3, Gfap, Aif1, Itgam, Cd19, Sdc1, Cd3e, Cd4, Cd8a, Il2, Il2ra, Il10, Tnf, Il1b, Ifng, Il6, Nfkb1, Fas, Fasl, Ppih, Gapdh

Sham, Cas9 RNP, Cas9 AAV

Cd19: n/a
Il2: p=0.094
Fas: * p=0.018

22

Figure S10. Assessment of SauCas9 transgene expression and off-target editing *in vivo*.

A) Next-generation sequencing (NGS) results evaluating indels at seven selected sites predicted as potential off-targets by Cas-OFFinder for SauCas9 RNP, AAV, and sham treated mice 28-days post-injection. No significant differences were found.
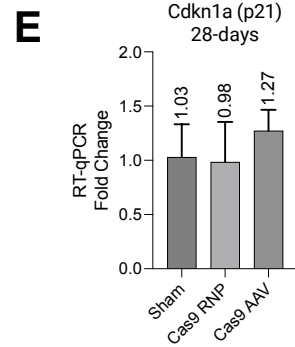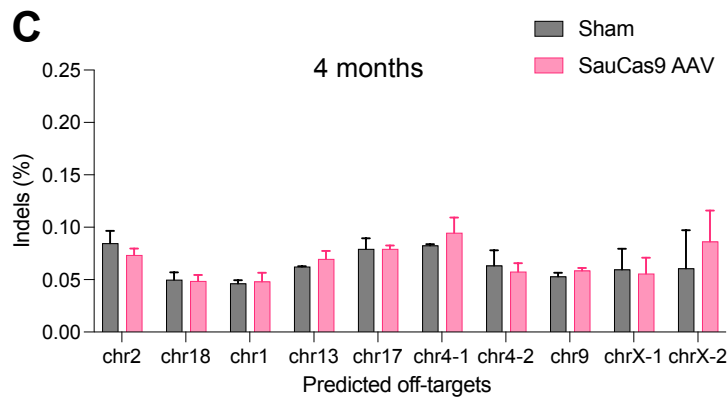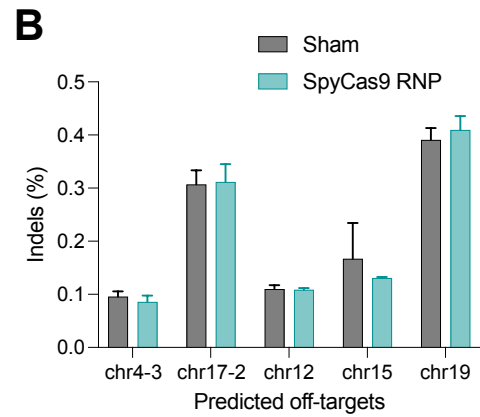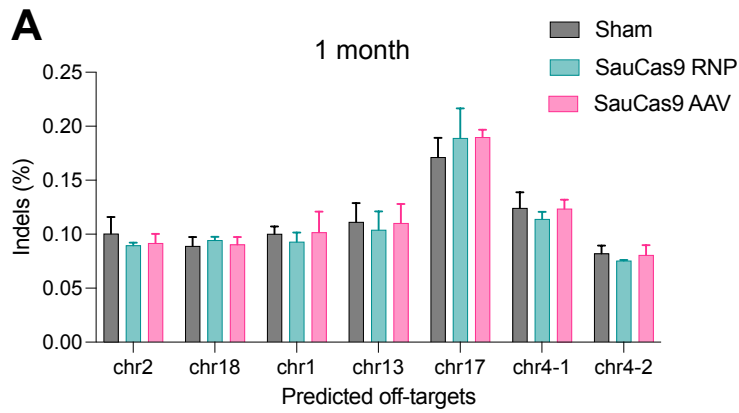
B) NGS results evaluating indels at five selected sites predicted by Cas-OFFinder for SauCas9 RNP and sham treated mice 28-days post-injection. No significant differences were found.

C) NGS results evaluating indels at ten selected sites predicted as potential off-targets by Cas-OFFinder for SauCas9 AAV and sham treated mice 4-months post-injection. No significant differences were found.

D) Digital droplet PCR assay for on-target indels at 4-months post-treatment (pink diamonds, right y-axis, maximum 2.2% in SpyCas9 RNP and 5.67% in SauCas9 AAV). Of note, a different lot of AAV9-SauCas9-sgRNA was in the 1-month experiments (Supplemental Figure 5G). SauCas9 expression was detected 4-months post-treatment only in the Cas9-AAV group (black circles, left y-axis, maximum 875 copies/ng), which correlated with indels. SauCas9 expression was not evaluated in the SpyCas9-RNP group. The result of the ddPCR (copies/μL) was multiplied by the total ddPCR reaction volume and divided by the cDNA input volume to calculate cDNA copies/μL. Then values were multiplied by the cDNA dilution factor, multiplied by the reverse transcription reaction volume, and divided by the starting amount of RNA (500 ng) to calculate copies/ng RNA.

E) No significant activation of p21 (Cdkn1a) was found via RT-qPCR at 28-days post-treatment with Cas9 RNP or Cas9 AAV.

F) Gene expression heat map showed significant upregulation of Fas in the Cas9 AAV group 4 months post-treatment with Cas9 AAV (n=4, unpaired t-test compared to sham, *p<0.05). Cd19 was not detected (n.d.) in the Cas9-AAV group.
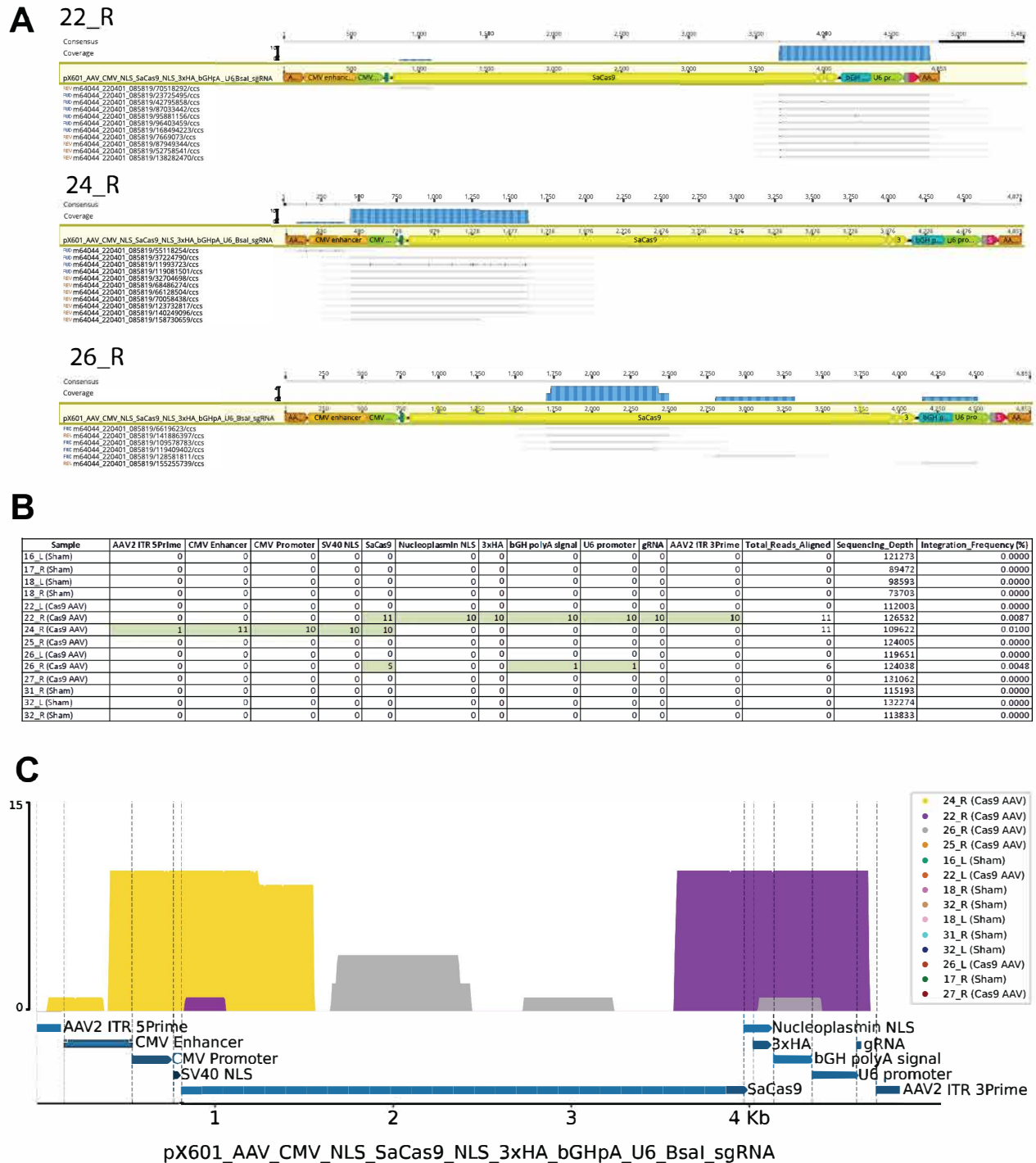
A

22_R

24_R

26_R

B

Sample	AAV2 ITR 5Prime	CMV Enhancer	CMV Promoter	SV40 NLS	SaCas9	Nucleoplasmin NLS	3xHA	bGH polyA signal	U6 promoter	gRNA	AAV2 ITR 3Prime	Total_Reads_Aligned	Sequencing_Depth	Integration_Frequency [%]
16_L (Sham)	0	0	0	0	0	0	0	0	0	0	0	0	121273	0.0000
17_R (Sham)	0	0	0	0	0	0	0	0	0	0	0	0	89472	0.0000
18_L (Sham)	0	0	0	0	0	0	0	0	0	0	0	0	98593	0.0000
18_R (Sham)	0	0	0	0	0	0	0	0	0	0	0	0	73703	0.0000
22_L (Cas9 AAV)	0	0	0	0	0	0	0	0	0	0	0	0	112003	0.0000
22_R (Cas9 AAV)	0	0	0	0	11	10	10	10	10	10	10	11	126532	0.0087
24_R (Cas9 AAV)	1	11	10	10	10	0	0	0	0	0	0	11	109622	0.0100
25_R (Cas9 AAV)	0	0	0	0	0	0	0	0	0	0	0	0	124005	0.0000
26_L (Cas9 AAV)	0	0	0	0	0	0	0	0	0	0	0	0	119651	0.0000
26_R (Cas9 AAV)	0	0	0	0	5	0	0	1	1	0	0	6	124038	0.0048
27_R (Cas9 AAV)	0	0	0	0	0	0	0	0	0	0	0	0	131062	0.0000
31_R (Sham)	0	0	0	0	0	0	0	0	0	0	0	0	115193	0.0000
32_L (Sham)	0	0	0	0	0	0	0	0	0	0	0	0	132274	0.0000
32_R (Sham)	0	0	0	0	0	0	0	0	0	0	0	0	113833	0.0000

C

pX601_AAV_CMV_NLS_SaCas9_NLS_3xHA_bGHpA_U6_BsaI_sgRNA

Figure S11. Long-read sequencing to detect viral fragment integrations at tdTomato locus following genome editing. A) Screen captures from Geneious software showing reads aligned to AAV reference genome (dark gray) with endogenous flanking regions (light gray) indicating viral genome trapping at tdTomato locus.
B) Tabulated reads from PacBio CCS within tdTomato locus that mapped to AAV genome components. The number of mapped reads was low (< 0.01%), however estimated on target editing by ddPCR was <10% of alleles (Supplemental 8D).
C) Visualization of reads mapping against the AAV genome. 3/7 sequenced brain samples that were injected with Cas9-AAV9 had detectable integration events, while 0/7 sequenced sham samples had detectable integrations.
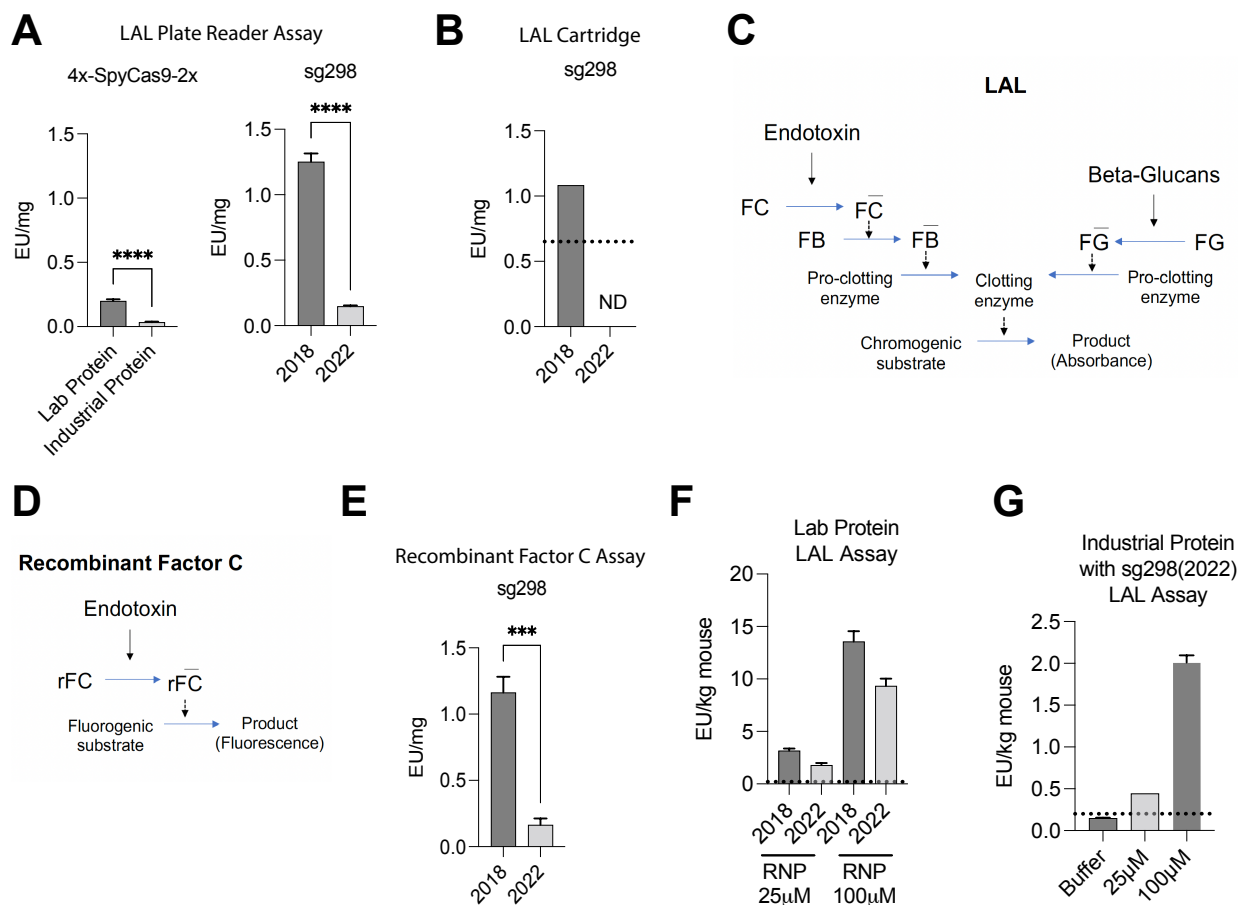
Figure S10. LAL and Recombinant Factor C assays to quantify endotoxins in RNPs.

A) Limulus amebocyte lysate (LAL) plate reader based assay (Endosafe, Charles River) was performed on two lots of 4x-SpyCas9-2x protein and two lots of sg298, compared to a control standard endotoxin (CSE) from E.coli 055:B5 to generate endotoxin units (EU) per miligram (mg). Samples were run in triplicate and analyzed with unpaired t-tests, **** p<0.0001.

B) LAL assay was repeated using the cartridge based system (Endosafe nexgen-PTS, Charles River), which reports a single value from two replicates with and without CSE spike-in internal controls. Statistical test was not performed. ND = not detected, dotted line represents limit of detection for the cartridge.

C-D) Schematic demonstrating the limulus amebocyte lysate (LAL) and recombinant factor C assays. The Recombinant Factor C assay has a fluorescent read out, negates the need for horsehsoe crab blood, and is not impacted by beta-glucans.

E) Recombinant Factor C assay (Pyrogene, Lonza) was performed on two lots of sg298 compared to a control standard endotoxin (CSE) from E.coli 055:B5 to generate endotoxin units (EU) per miligram (mg). Samples were run in triplicate and analyzed with unpaired t-tests, *** p<0.001.

F) Final RNP formulation (laboratory 4x-SpyCas9-2x protein with sg298 lots) had significantly more endotoxin than the FDA recommendation of 0.2 EU/kg/hr (dotted line) for human drug products administered into the central nervous system when delivered at 10μL in a 22g mouse.

G) The optimized RNP formulation (industrial 4x-SpyCas9-2x protein with sg298 from 2022) nearly reached the FDA recommendation of 0.2 EU/kg/hr (dotted line) at the 125pmol dose (25μM). Given the linear increase between 25-100μM the 10μM dose (50pmol) may be sufficient to reduce endotoxin below the threshold, while maintaining high levels of editing.
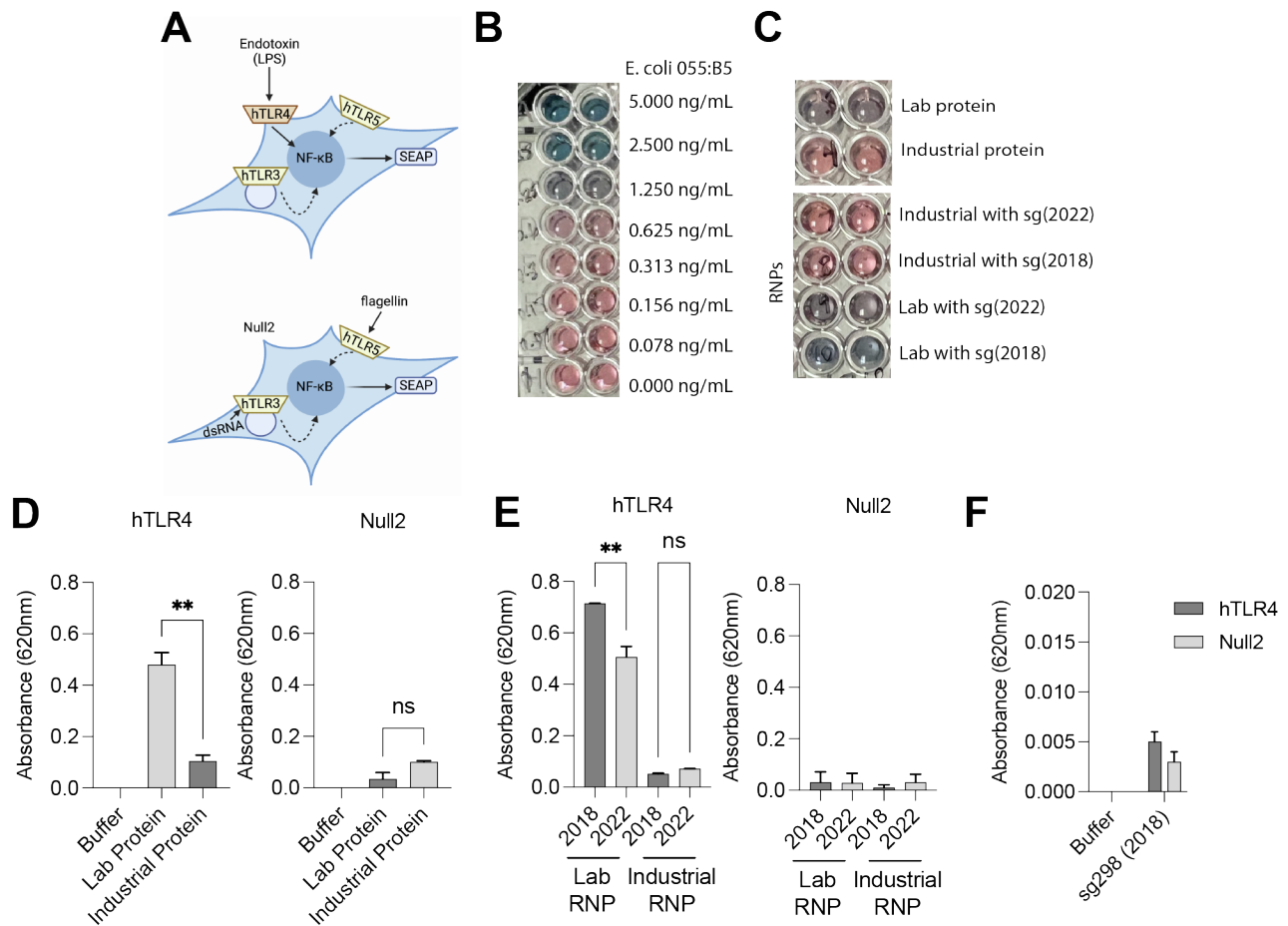
Figure S13. The effect of endotoxin in RNPs on NF-kB activation measured via HEK-Blue assay.

A) HEK-Blue Assay (InvivoGen). Stimultaion with a TLR4 ligand, such as endotoxin / LPS, activates NFkappaB and AP-1, which induces secreted embryonic alkaline phosphotase (SEAP). SEAP can be easily detected in the cell-culture media and read with a plate reader. The parental cell line, Null2, will produceSEAP in response to TLR3, TLR5, and NOD1 agonists and is used to control for TLR4-specific activation of NFkappaB/AP-1.

B) Representative images of blue media change due to SEAP release downstream of NFkappaB/AP-1 activation following stimulation with control standard endotoxin.

C) Representative images of blue media change due to SEAP release downstream of NFkappaB/AP-1 activation following treatment with proteins and RNPs.

D) HEK-Blue Assay applied to proteins made in the lab or industrial scale-up. The lab-produced protein induced significantly more SEAP than the industrial protein. Assay was run in duplicate, unpaired t-tests, ** p<0.01.

E) HEK-Blue Assay applied to RNPs made with lab or industrial protein and sg298 from the 2018 or 2022 lots. The lab protein with the sg298 ("standard" formulation) was the most potent at inducing SEAP, while cells treated with the the industrial RNPs had much less SEAP production. Assay was run in duplicate, unpaired t-tests, ** p<0.01.

F) HEK-Blue assay applied to sg298 (2018) lot showed minimal change in absorbance from buffer. Assay was run in duplicate. Cells treated with sg298 lot from 2022 alone was not included in this experiment.

A

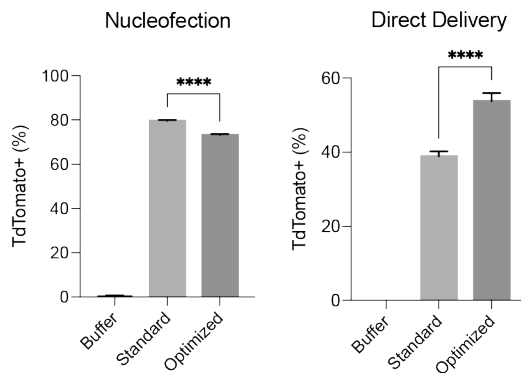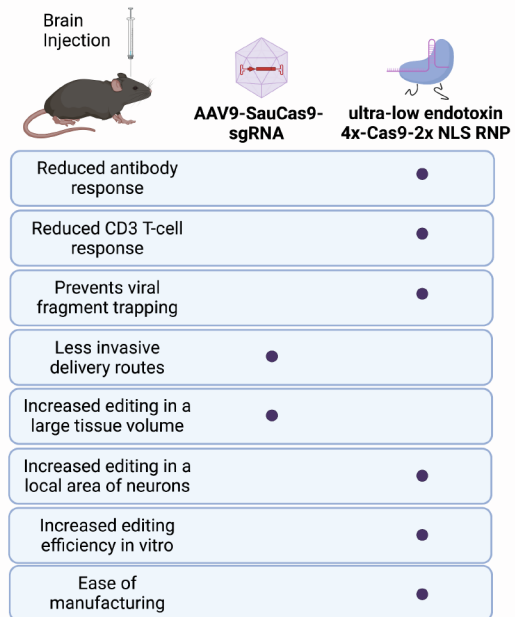| RNP	Guide RNA	Protein
Standard	sg298 (lot 2018)	4x-Cas9-2x NLS (Laboratory prep, low ET)
Optimized	sg298 (lot 2022)	4x-Cas9-2x NLS (Industrial ultra-low ET)

B

Figure S14. In vitro testing of optimized RNPs and final summary.

A) Optimized RNPs (ultra-low endotoxin (ET) industrial protein with sg298 from 2020 lot) edited fewer Ai9 NPCs via nucleofection and more NPCs via direct delivery compared to the same dose (100pmol) of standard RNPs. This result showed similar trends to increasing the number of NLS on the N-terminus of SauCas9, suggesting more cell-penetrating peptides improve self-delivery / endosomal escape and reduce nucleofection efficacy (likely due to positive charge mechanism). These differences could also explain in-part the measured difference with editing in vivo (Figure 3), although the optimized RNPs were at least as efficacious in vivo as the standard formulation (Figure 1), demonstrating potential lot-to-lot variability in potency (active site concentration). Protein concentrations were confirmed via nanodrop before both in vitro and in vivo experiments.

B) Comparison of AAV9 and 4x-NLS RNP mediated delivery of Cas9 in the mouse central nervous system. To enable high-levels of editing in neurons within a localized brain region, minimize adaptive immune responses, and timely and affordable manufacturing scale up, the RNP offers an effective alternative delivery system to viral vectors. Image made using Biorender.com.